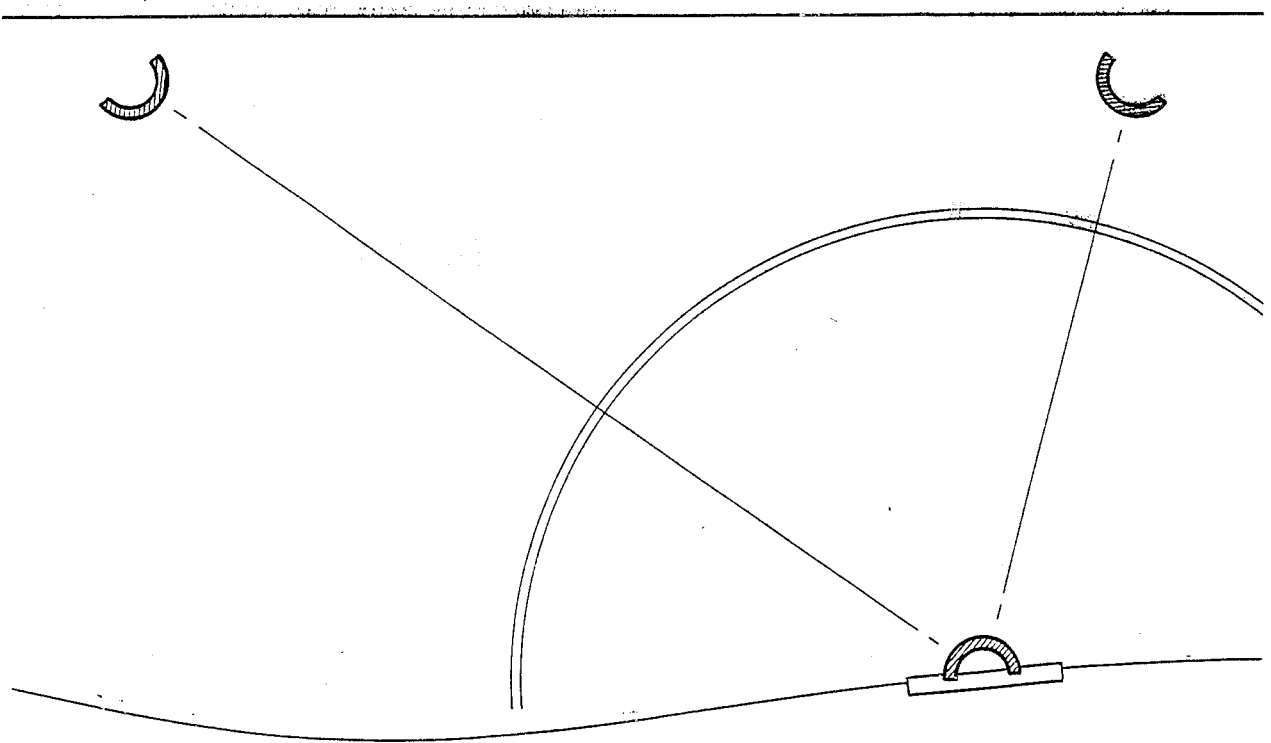


Edinburgh Wave Power Project



DEVELOPMENT OF SONAR RANGING TECHNIQUES FOR
THREE DIMENSIONAL MEASUREMENTS IN MIXED SEA BASINS

SERC Grant No GR/D/8426.9

D J Rogers

August 1987

EDINBURGH UNIVERSITY WAVE POWER PROJECT

University of Edinburgh

Mayfield Road

Edinburgh EH9 3JL

031 667 1081 Ext 3276

CONTENTS

	Page
1 INTRODUCTION.....	2
2 OBJECTIVES	3
3 MAIN CONCLUSIONS	4
4 WAVE GAUGE BUOY AND MOORINGS	6
5 SONAR DETECTION AND ELECTRONICS	12
6 POSITION MEASUREMENT	22
7 WAVEGAUGE EVALUATION	27
8 SPECIFICATION OF SONAR MEASUREMENT SYSTEM	36

APPENDICES

I POSITION CALCULATION	40
II ERRORS DUE TO WAVE MOTION	43
III TWO PLANE WAVE SOLUTION FOR SINGLE WAVEGAUGE	46
IV CIRCUIT DIAGRAMS	49

PHOTOGRAPHS

	Opposite Page
BUOY AND MOORINGS	11
COMPLETE ELECTRONICS	26

1) INTRODUCTION

There is an interesting lexical gap in the English language. We measure, talk of, draw and photograph the vertical height of waves but never the horizontal movement. Even the highly specialised nautical vocabulary contains no word equivalent to *surge* and *sway*. For the circular orbits of regular, uni-directional, deep-water waves this omission (and the mental blockages that derive from it) cause few problems because the single horizontal motion will be the same as the vertical one. But in shallow water, or multi-directional irregular spectra, or in tanks with reflections and cross waves, the two horizontal axes can be just as interesting as the vertical one. Indeed horizontal fluid loading is often about double that in the vertical direction for floating objects with cross-sectional aspect ratios close to unity.

The purpose of this project is to develop a working instrument for use in model test tanks which will allow the convenient measurement of all three axes of water movement.

2) OBJECTIVES

Our plan was to mount a piezo-electric sonar transmitting device on a buoy and moor it so that it could follow local water movement but not be moved off station by surface currents. Its signals would be picked up by three microphones on the tank floor.

The dimensions of the buoy had to be chosen to provide the necessary load-bearing capacity, but not at the expense of high-frequency response. Errors from pitch and roll had to be eliminated.

The driving and receiving circuitry had to give unambiguous time signals with the minimum of jitter despite any variations in the signal level.

The three time-interval measurements had to be converted by trigonometrical calculation to provide output in more conventional XYZ axes.

Finally the waterproofing of the underwater parts had to be exceptionally sound.

3) MAIN CONCLUSIONS

- (1) Piezo-electric sonar transducers can provide an excellent three-dimensional wave gauge.
- (2) A suitably moored buoy with a diameter of 50 mm can follow water movement to an accuracy of $\pm 1\%$ of wave size at frequencies up to 1.4 Hz and give useful information ($\pm 10\%$) at frequencies up to 2.5 Hz.
- (3) The time-constant of the return to mid position following an offset in calm water is 3.5 seconds with no overshoot. This indicates a large damping relative to the velocity of the water and good performance at frequencies far below those of interest at 1/100th scale.
- (4) Wave tanks are acoustically quiet at high frequencies and so it is possible to use edge-triggered timers rather than the conventional packet triggering. We are able to get the jitter down to 10 nanoseconds - nearly three orders of magnitude down on a typical packet length.
- (5) The resolution of the instrument can be improved by pre-shaping the drive pulse and is considerably better than our target of 0.1 mm. We will be able to modify the circuitry to resolve 0.025 mm - about the resolution of an engineering vernier gauge - in a tank 1.2 m deep.
- (6) It is necessary to use two carefully chosen floats and weights for each of the three mooring lines. With proper design of line length the fluid forces on the lines can improve the accuracy of the float movement. The final assembly is rugged enough to be permanently fitted in a wave tank but careful planning and a dummy buoy are necessary if the installation process is to avoid entangled lines.
- (7) The repetition rate of the sonar pulses is fast enough for time-sharing among a number of transmitters. Three transmitters could determine all six degrees of freedom of a ship model.

- (8) The timing circuitry can accept a wide range of amplitude variations. This means that ship models could be tracked anywhere in a tank with a fairly cheap array of microphones. This could prove to be just as useful as wave measurement. The range could easily be as much as 50m.
- (9) The absolute accuracy of the instrument is affected by the movement of the water through which the sound is passing. The magnitude of this error is less than 0.2% and could in principle be corrected by software.
- (10) The trigonometrical calculations necessary to extract XYZ positions can be performed in real time by a small microcomputer such as the BBC model B. Some simplification results if the microphones lie in a plane perpendicular to the Z axis.
- (11) The instrument has already proved its use for the detection of small reflections and cross waves in regular seas, for which the maximum likelihood method with a cluster of vertical gauges gives unpredictable results.

4) WAVE GAUGE BUOY AND MOORINGS

The conflicting aims in 3D wave gauging are for the buoy to follow the motion of a water particle on the surface while remaining within the same area. The presence of drift forces makes this impossible, so there must be restraining moorings, as well as wires to bring the signals into the transducer.

The ideal shape for the buoy is hemispherical and the graph in Fig 4.1 shows the wave-following properties for such a shape with diameter d in a wave field of angular frequency w and gravitational field g . There is a resonance when $w^2d/g=2$, so the buoy should have a diameter of less than g/w^2 for all useful frequencies, and less than half this value where accuracy is required.

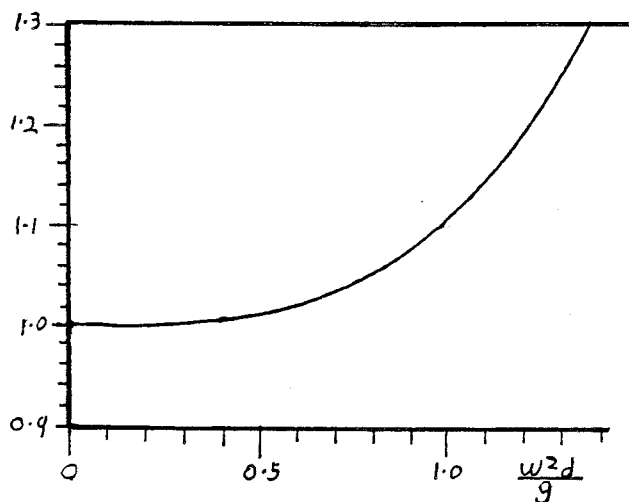


Fig 4.1. The ratio of buoy to wave motion for a floating hemisphere.

Our minimum requirement was for a sonar gauge accurate to 1% up to 1.4Hz and able to operate to 2.5Hz. A buoy of 50mm diameter fulfils this requirement. Because the moorings and wires impose a viscous drag load on the buoy which opposes the effect of its resonance, the buoy can be expected to follow the water motion more closely than this prediction. The buoy must support the weight of the piezo transducer, the material above the waterline, the mooring lines and connecting wires. As the void space inside the buoy is limited by the hemisphere dimension, there is a minimum buoy size which will stay afloat while keeping the transducer at its centre.

To prevent the pitching and rolling motions of the buoy from affecting the apparent position, the transducer must be at the centre of the buoy body, as shown in Fig. 4.2. The water surface acts as reflector and so the

hemisphere is able to produce a spherically symmetrical sonar signal. To enable this signal to disperse from the piezo element, it is necessary either to make the buoy of a material, like polypropylene, that is transparent to the sonar signal, or to cut the buoy away to leave three webs beneath the water, with clear apertures for the sonar signal.

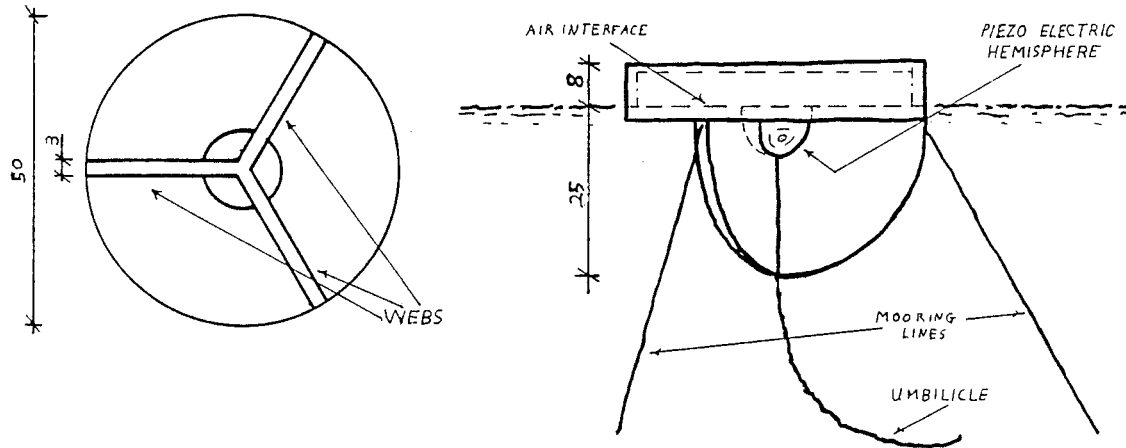


Figure 4.2. Views of the webbed buoy from the side and below.

The moorings were designed using the assumption of linear wave theory ignoring the non-linear viscous drag effects. The first set of moorings consisted of three sets of floats and sinkers, as shown in Fig 4.3a.

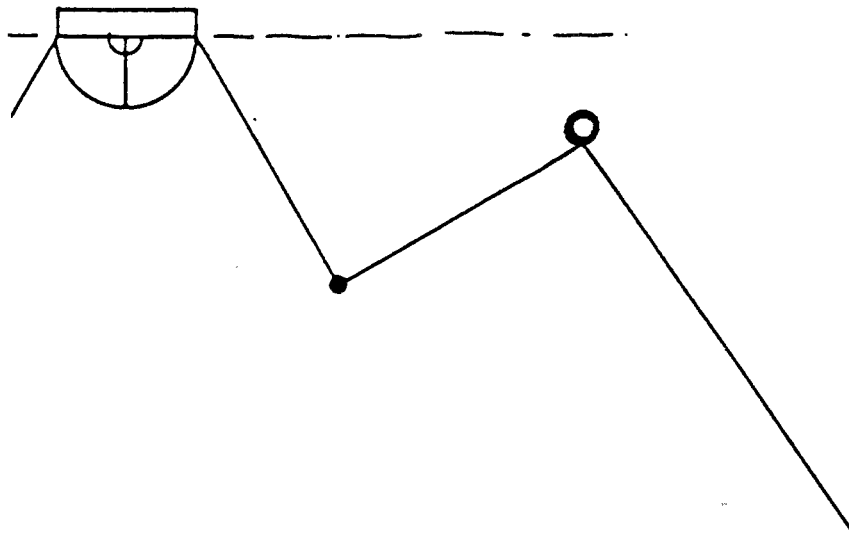


Figure 4.3a. One leg of the first mooring which was unsatisfactory at high frequencies.

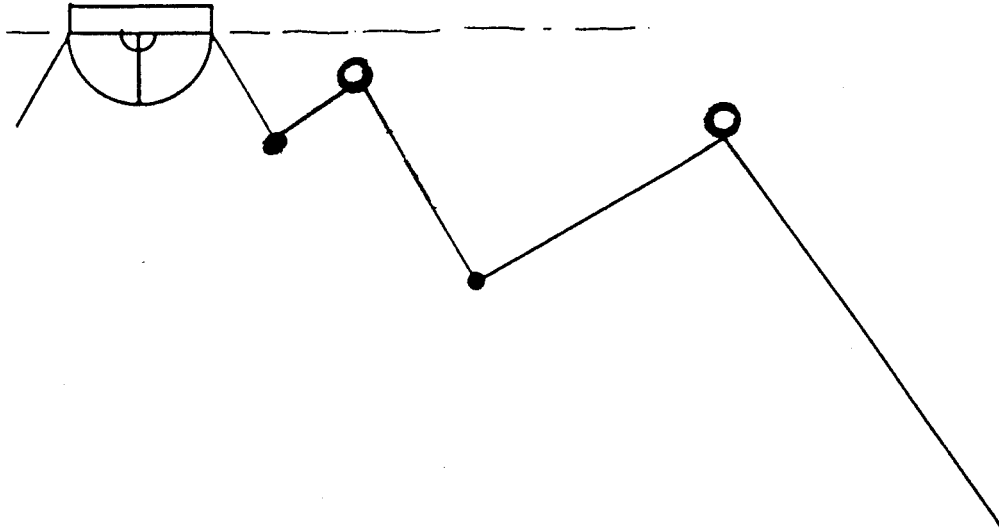


Figure 4.3b. The improved duplex sinker/float combination.

This arrangement puts a spring centralising force on the buoy that is linear to within a few percent over half a metre range. It was found that while this arrangement allows large motions at low frequency it imposes too great a load on the buoy at high frequencies, when the effective length of the mooring lines acting on the buoy is too long. The arrangement was redesigned using a double float sinker geometry, shown in Fig. 4.3b, which increases the frequency range.

The sinkers act as simple inertias while the larger volume of the floats gives them an added mass equal to their buoyancy that makes them try to follow the water motion. If a float is close to the surface and the buoy and float move in near unison, float movement will not corrupt the buoy movement. However, if the distance from the buoy to a float is more than a small fraction of a wavelength, the water motion at the float will be out of phase with that at the buoy and forces on the float will reduce the accuracy of buoy movement. A compromise can be achieved by putting the float sufficiently far below the surface that the shorter, out of phase waves are attenuated. The float depth was chosen so that the water motion around it should be halved when the distance to the buoy was a quarter of a wavelength. The final positions of the floats and sinkers, shown in Fig 4.4, were found by observation of their motions in a variety of waves.

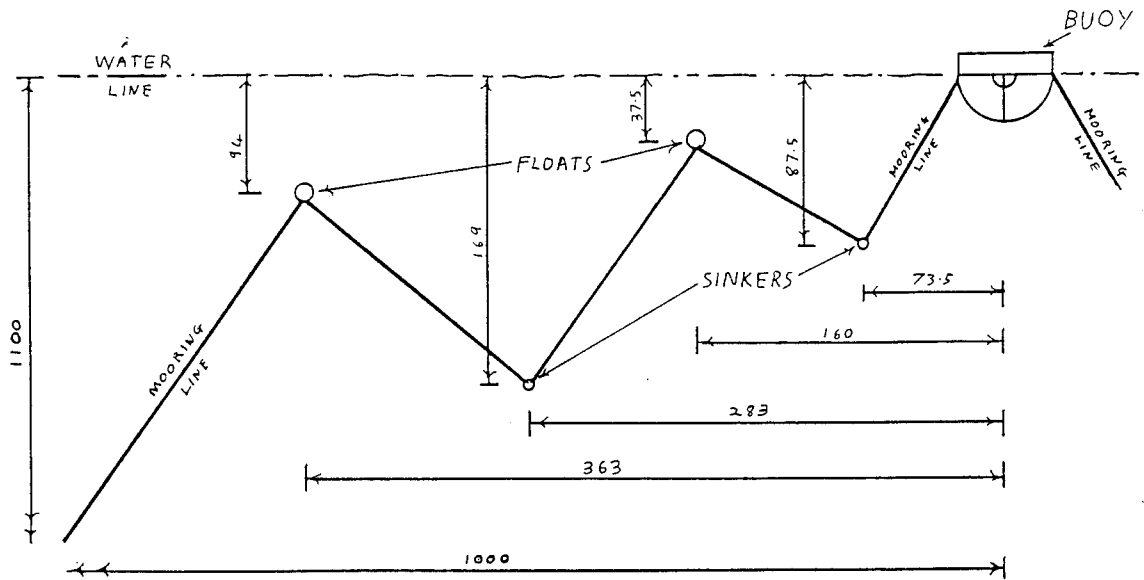
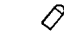



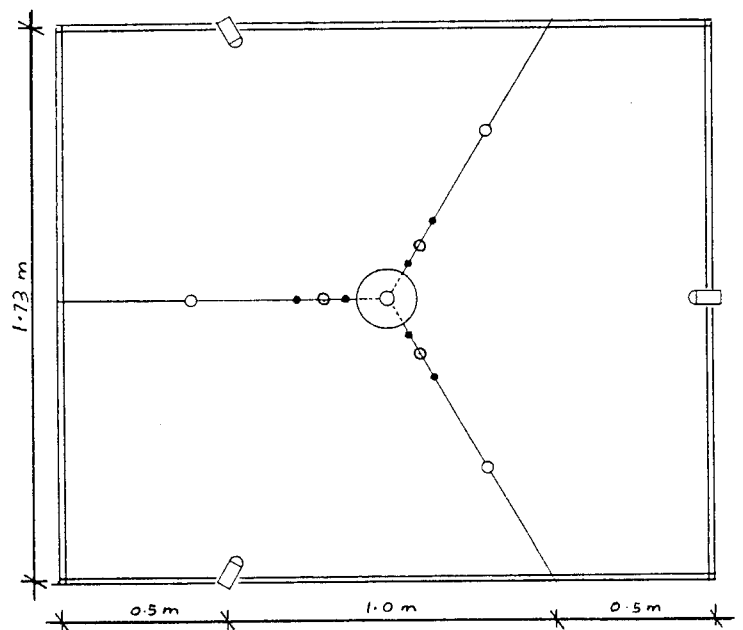


Figure 4.4. The final dimensions of the mooring. Sinker weight and float buoyancy were both 0.7 grammes. The lines had a breaking force of 5 Newtons.

With this design the sinkers oscillated from side to side and the roll motion of the buoy was easily excited. By fixing the moorings to the rim of the buoy and by flattening the weights in a vertical plane we were able to damp the oscillations. The final design used the thinnest fishing line available (breaking tension = 5 N), and two lead shot with a combined weight of 0.7gms to act as sinkers, with floats trimmed to support one weight exactly. The receivers and mooring points were anchored to a rectangular frame on the tank floor, shown in Fig 4.5.

Fig 4.5. A plan view of the mounting frame showing moorings and receiver locations.

- Receiver - 
- Float - 
- Sinker - 
- Buoy - 



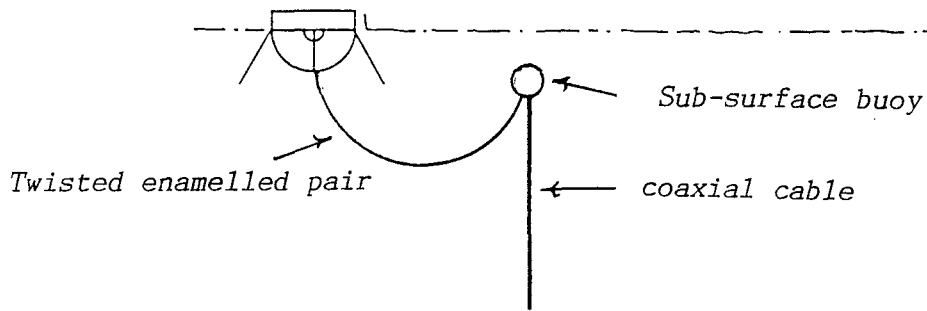
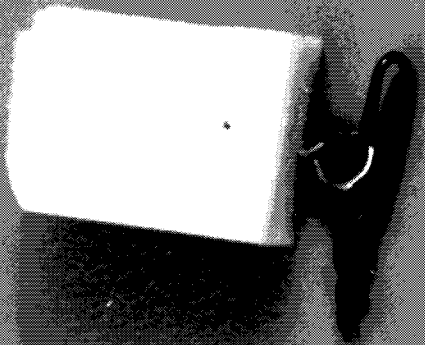
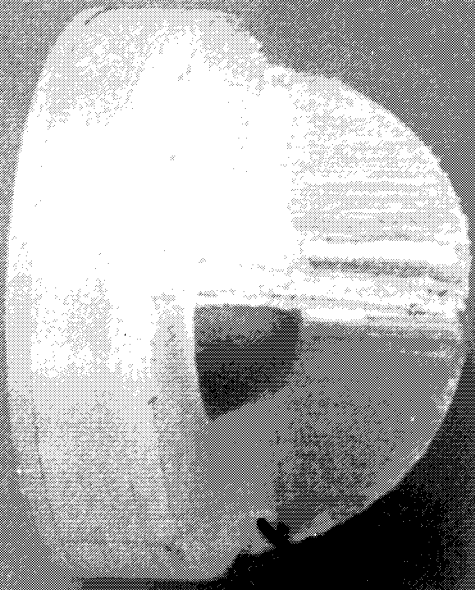


Figure 4.6. Details of the electrical cable attachment.

Bringing electrical signals to the buoy is difficult. All coaxial cables proved to be excessively stiff, so twisted pairs of wire were tried. These were joined to a coaxial cable that rose from an anchor weight at the bottom of the tank to a subsurface buoy, as shown in Fig 4.6, and then formed a catenary entering the buoy at its base. The most flexible wire available still imposed a loading on the buoy that was easily discernible. We therefore constructed our own cable from two strands of enamelled copper wire 0.06mm diameter. These were twisted together and coated with silicone rubber by extrusion through the needle of a hypodermic syringe.

The moorings were fragile when handled out of the water. But with the use of quick-release hooks at the end of each line and a dummy buoy it was quite easy to deploy the mooring lines. It was then possible to manoeuvre the anchor weight at the bottom of the coaxial cable so that the subsurface buoy was upwave and to one side of the final position of the sonar-transmitting buoy. Then the moorings could be transferred to the sonar buoy.



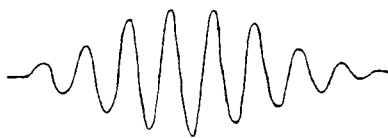
Standard at 20°C

10 20 30 40 50 60 70 80 90 100

The photograph shows a hemispherical piezo element at the centre of a webbed buoy with the nearest sinker and float. Fishing technology provides an excellent source of weights and quick line connections.

5) SONAR DETECTION AND ELECTRONICS

The speed of sound in water is a little less than 1.5 Km per second. To resolve to within 0.1 mm requires the transit time of the sonar wave train to be timed to within 1/16th of a microsecond. The resonant frequency of a hemispherical piezo transducer is proportional only to its diameter. With the smallest device, of 12.6 mm diameter, this corresponds to a maximum frequency of 150 Khz. To achieve adequate precision the electronics must be able to resolve to better than 1/100th of a sound wavelength. Sonar packets are about ten wavelengths long (Fig 5.1a), and normally the nominal centre of the packet is detected. This technique is employed for measuring the direction of a sonar transmitter, using closely spaced receivers. Such information is not sufficient to define range exactly, but the use of two or more frequencies could overcome this. Because of the problems of reflected waves interfering with the direct path wave and the problems associated with creating two independent frequency pulses the double frequency technique was rejected. The resolution requirement necessitated the use of a technique that more precisely identified the centre of the wave packet.



*Typical sonar
packet*

Fig 5.1a



*Auto-correlator
output*

Fig 5.1b



*Compressed sonar
packet*

Fig 5.1c

Radar systems have achieved this by using correlation techniques. One of these uses a signal that rises in frequency through the packet. This "chirrup" is then detected using a delay-line auto-correlation filter. The typical output would then be as in Fig 5.1b with a pulse width of between a half and one period. Normally in radar applications this pulse would be detected directly. Techniques can be used to define more precisely when the event happened, either by observing the rising and falling zero-crossing points or by working with the zero crossing of the differential.

A simpler route is to shorten the wave train effectively to one wavelength. This allows a single zero crossing to be identified, so providing the accuracy we require. In practice a waveform similar to Fig 5.1c is seen. To create a wave of this form requires control of the drive pulse and impedance matching of the sonar transducers to control their resonance characteristics. The ability to detect a particular trigger-arming peak prior to the chosen zero crossing is the heart of this technique. Whereas correlation methods use information from the entire packet and so have good noise rejection, edge detection methods are very sensitive to noise. However we found that the tank background noise was very low. At a range of 3 metres the detection signal levels are large and the signal-to-noise ratio is high.

In order to detect the peak prior to the designated zero crossing, several features are required of the pulse at the receiver. In Fig 5.2a the wave train is compared with a value that is some fraction of the maximum peak value detected from a previous pulse. In order not to detect the pre-peak, while unambiguously detecting the main peak, it is desirable for the ratio between them to be greater than four. This allows for errors in the detection level and variation from sample to sample, as well as noise. It is equally important for the post-peak to be limited in amplitude. Ideally it should be lower in amplitude than the main peak. The suppression of the post peak and subsequent ringing reduces the acoustic noise in the tank that could interfere with the signal from other transmitters.

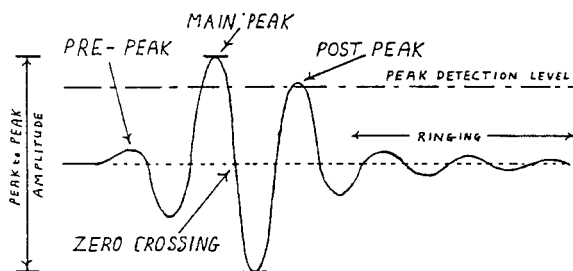


Fig 5.2a. Features of a sonar pulse.

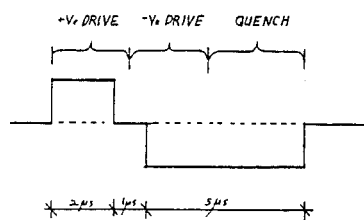


Fig 5.2b The drive pulses for the best received signal

Piezo transducers are not perfectly matched to the water and tend to have a high "Q". By using hemispherical transducers that produce a good radial sonar field the resonant frequency is well defined. As identical devices were employed for transmitter and receivers the impulse was double filtered by the time it reached the receivers. This filtration was further improved by impedance-matching the drive amplifier and by fitting damping resistors to both transmitting and receiving piezo elements. We used a 2 microsecond i.e. 1/3rd wavelength pulse. We found that if we drove the transmitter high in one half cycle and low for the next, the resultant signal at the receiver could be made more than twice as large with no degradation of the peak detection ability. By extending the second pulse, as shown in Fig 5.2b, the post peak can be reduced in amplitude and the ringing of the transmitter can be greatly reduced.

The wave shape obtained from the complete transmitter/receiver assembly is given in Fig 5.3a. This signal suits the requirements of the detector, with a post-peak smaller than the main peak and a pre-peak very much smaller. The frequency analysis of this wave is given in Fig 5.3b. This shows that there are significant components down to 50 kHz and up to 300 kHz. Filters were optimised to reduce front-end noise. The main problem was the phase shifting of the various critical components of the waveform.

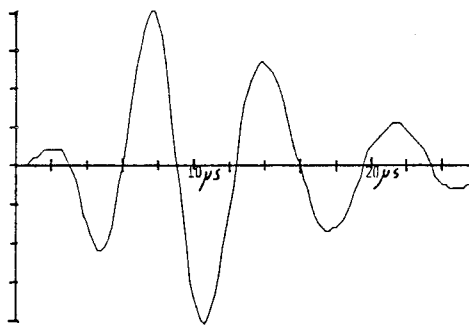


Fig 5.3a. The sonar packet at the receiver.

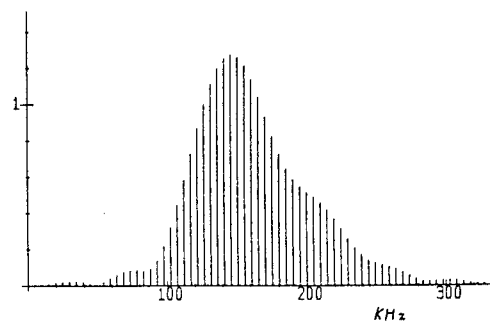


Fig 5.3b The spectrum of the received signal.

The final design consisted of a critically damped second-order low-pass filter with a break-point frequency of 325 kHz, and two first-order high-pass filters set to about 15 kHz. This gives an effective noise bandwidth of 360 kHz. In terms of overall signal-to-noise ratio there was little to

be gained in narrowing the filters, as the amplitude of the post-peak tended to increase. When the complete system with optimised filters was tested, it was found that in some circumstances the post-peak became larger than the main peak by up to 20%. The pre-peak was always less than 1/9th of the amplitude of the main peak so a peak detection level 1/3rd of the stored peak value was practical.

The front end pre-amplifier is a ZN460, adjusted to give an impedance of 150 ohms. This matches the receiving piezo element which has an impedance between about 100 ohms and 200 ohms over the bandwidth. Signals measured on the final system show front-end noise of 3 μ Vrms or peak noise of about 10 μ V. The receiver gain is 1000 and so, by setting the maximum and minimum peak amplitude to 0.6 volts and 9 volts respectively, the signal-to-noise ratio is kept better than 60/1. This gives a worst case jitter of 10 ns rms while allowing a dynamic range of 15 to 1. The 16 MHz counters are started synchronously with the transmission pulse. Low power Schottky TTL is used for the counter and the discrimination logic. The transmitter pulse is sent to the transmitter driver by a line driver, and the clock and associated signals, shared by a number of boards, are buffered using FAST TTL. The zero crossing comparator was chosen for its predictable delay time. It was thought that this design would have an overall jitter specification less than 30 ns, which would represent half a bit.

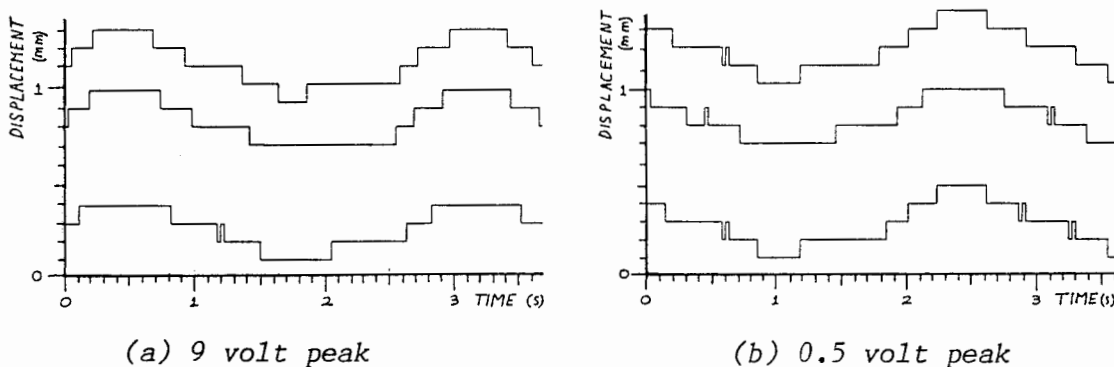


Figure 5.4. Displacement output signals in very small waves for high and low sonar signal strength. The wave amplitude was 0.2 mm in each case.

After the construction of a single transmitter/three receiver assembly, tests were carried out to determine the noise in the system. The transmitter buoy was placed in a 0.2 mm nominal amplitude wavefield.

Samples were then taken at 40 Hz, with one receiver and preamplifier feeding the three receiver boards in parallel. By supplying the transmitter drive circuit with different voltages, the noise tolerance at different signal amplitudes could be found. Figure 5.4 shows the output from these boards against time for two different signal levels. Because the electronics could resolve only 0.1 mm the sine wave signal is quantised into steps of this size. Between each state change there are 10 to 20 samples, so if the noise was 1/10th of a quantum interval we could expect uncertainty on the transition. But only one false edge was found over one hundred wave cycles with a drive of 9 volts (Fig 5.4a). The noise level is therefore well below a tenth of a quantum interval, possibly as low as 1 ns although this is below the jitter of any of our test instruments. A second test was performed with a peak signal level of 0.5 volts. In this case (Fig 5.4b) noise on the transitions can clearly be seen. A noise figure of 1/10th of a bit can be assumed at this reduced signal level, representing an overall jitter of 6 ns rms. This is a factor of five better than we predicted.

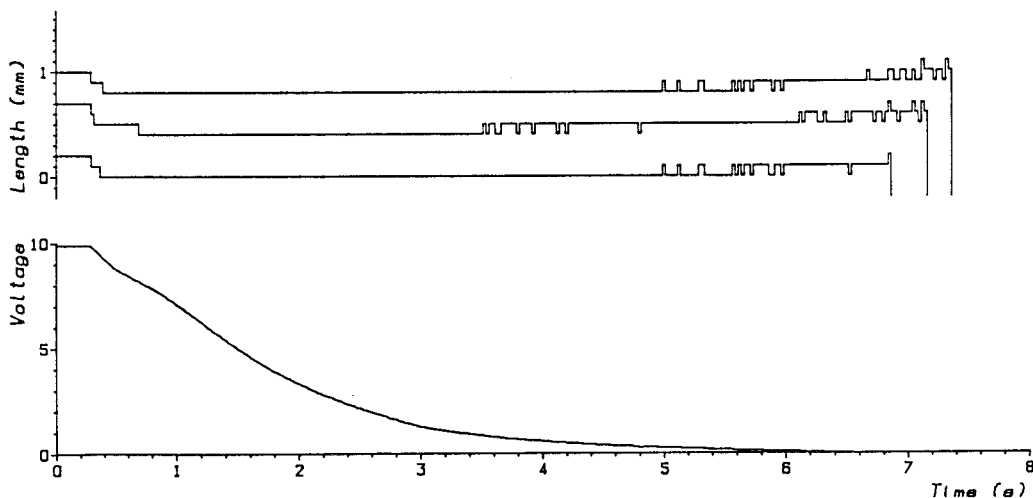


Figure 5.5. Displacement outputs with a slowly decaying drive signal demonstrating the width of the dynamic range.

A further test was carried out to find the variation of output with signal level. The power supply to the transmitter drive circuit was disconnected and the supply voltage allowed to decay naturally. Fig 5.5 shows the decaying signal at the peak detector, and the outputs of the three edge

detectors. When the signal first decays, a change in position of two quantum intervals can be seen. This is due to the non-linearity of amplifiers performing close to their limiting slew rate which causes the zero crossing point to be shifted. The problem could be overcome by a reduction of the overall gain. As the signal decays below one volt peak, the output starts becoming noisy, but it is not until the signal falls below the resolution of the A-to-D converter that the circuitry fails to work. The output timing is therefore highly tolerant to variations of input signal levels.

A 16 bit counter driven at 16 MHz gives a range of 6 metres. This could easily be increased without degradation of signal quality by altering one resistor in the pre-amplifier or raising the transmitter drive voltage. The practical range limit for our present transducers is 50 metres and larger piezo elements could be used at ranges in excess of 100 metres.

The system was initially built using a 16 MHz clock, giving a resolution of 0.1 mm. This limit was imposed both by the capabilities of the TTL devices in the circuit and by the expected overall jitter figure of 30 ns. As the system tests exceeded expectations it was then decided to improve the resolution from 60 ns to 10 ns. Raising the clock frequency to 100 MHz would have required a total redesign around ECL devices. This would have been difficult and more expensive. Instead, an accurate multi-tap delay line was used to produce a family of six 8 MHz clocks delayed from each other by 10 ns, along with two phase-shifted 4 MHz clocks, as shown in Fig 5.6.

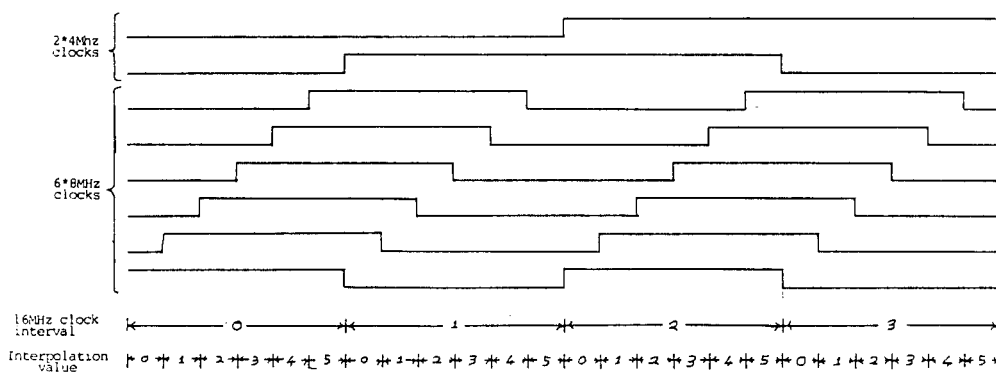
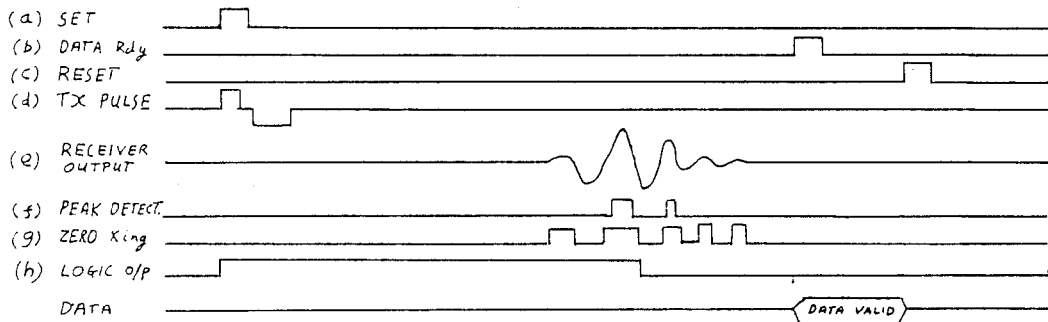
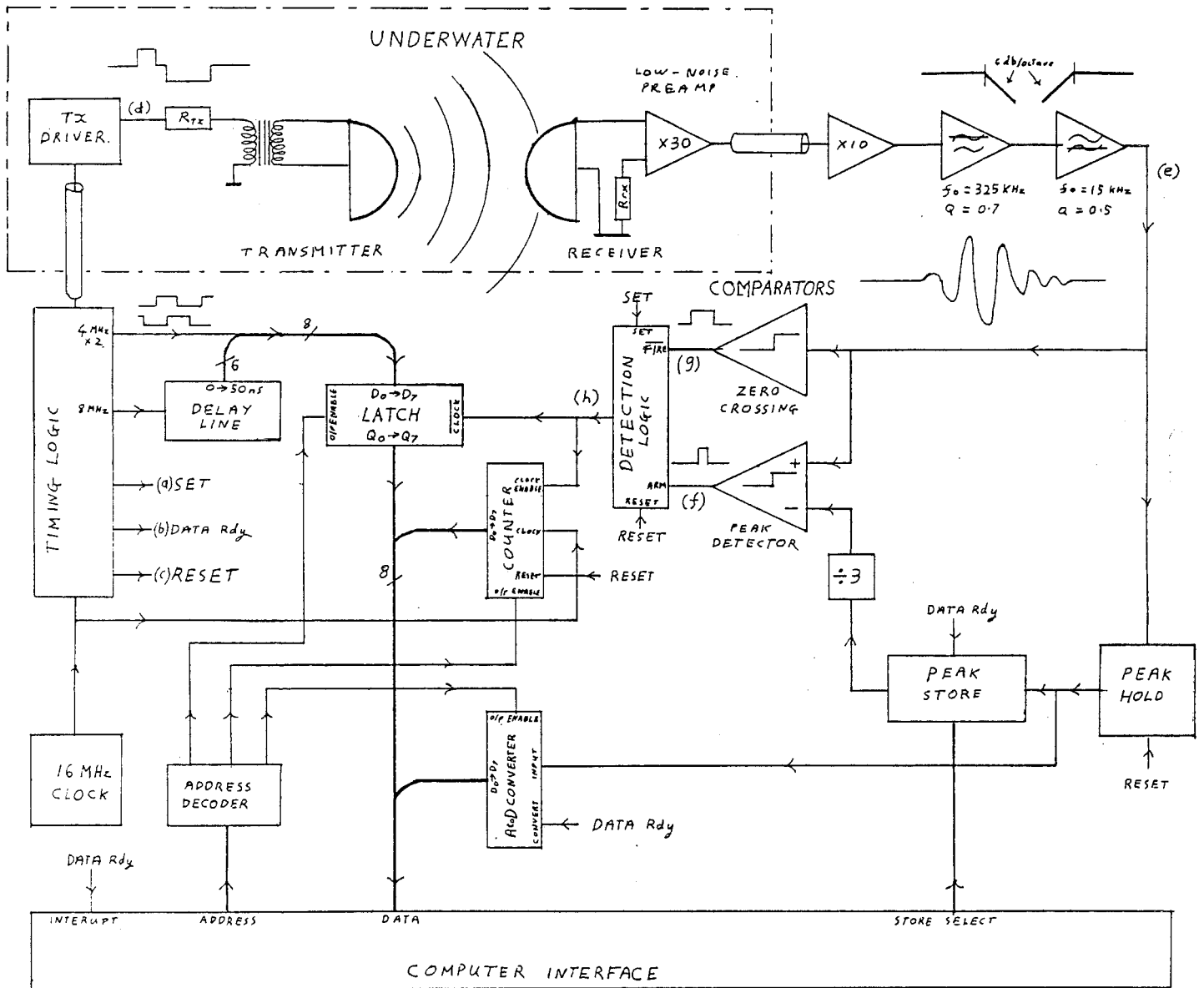


Figure 5.6. Phase-shifted clock signals prior to the receiver latch which provide increased resolution.

By freezing these clocks in a latch, the time within one clock cycle can be determined. This information then is tied in with the counter and, since the timing of these routes is different, an overlap of information is required to determine the final value. To achieve this we used the 9 MHz clock combined with the two phase-shifted 4 MHz clocks to give a two bit overlap. This allows a timing error between the two routes of 60 ns. In all the time-critical circuitry FAST TTL has been used. Also ground-planed backplane has been used throughout, with the critical signals terminated at the end of the backplane.

The block diagram in Fig 5.7 illustrates the main points of the system. For simplicity only one transmitter and receiver are shown. Where there are a number of transmitters or receivers the 16 MHz clock, the timing logic and the delay line would be common to them all. All other components are repeated as necessary, connected to a common computer interface. The timing logic ensures that the transmitter pulse is synchronised both with the start of counting of the counter and with the first rising edge from the delay line. The transmitter pulse is shaped and amplified by the driver which is situated close to the transmitting piezo-electric device. The transformer and load resistor matches the drive and ensures a drive signal of up to 100 volts peak-to-peak. The sonar packet is detected by the receiving piezo-electric device. This signal is impedance-matched by the load resistor and amplified by the low noise pre-amplifier placed underwater, close to the receiver, to avoid noise pickup. The signal is then robust enough to be transferred to the rack-mounted conditioning circuit. Here it is amplified further and filtered to reduce the noise. The final signal is then monitored to detect the significant zero crossing. To achieve this accurately, the significant peak is detected by comparison with the previously stored peak, attenuated to a third of its original value. The pulse from this comparator arms the detection logic so that the next zero crossing detected by the comparator triggers the detection logic, stopping the clock and freezing the status of the delayed clocks in the latch. The peak hold simultaneously follows the input signal and holds the maximum value detected within the current cycle. After the maximum allowed time, the value from the peak hold is used to update the peak store, and its value is converted, ready to be read by the computer. The computer is then informed that this has happened. It then reads the two bytes from the counter, followed by the status of the frozen phase-shifted clocks. It then



Typical signals at critical points in the circuit.

Figure 5.7. Schematic diagram of the main circuit elements.

combines them to compute a time accurate to the nearest 10 ns. The computer also tests the signal size and can reject readings that are due to echoes or distant transmitters triggered in a previous cycle.

To cater for a number of transmitters and receivers, the electronics has been designed into a number of modules that are linked by a common backplane as shown in Fig 5.8. Provision has been made in the design for up to 4 transmitters and 16 receivers. There are four card types and one terminator. The timing control card carries the master clock, the timing control logic and the delay line. It drives the master timing bus, and the multi clock bus. In order that these signals should not be distorted by impedance mismatch, the timing board must be positioned at one end of the ground-planned backplane, with terminating resistors at the other. The computer interface card can initiate a transmission sequence, so allowing it to lock this system to a remote sampling clock. In the implementation we used, the values from the receiver cards were then stored in memory ready for transfer to the host computer. The transmitter cards can handle up to two transmitter drivers, each with a board selectable address. More than one transmitter can be fired simultaneously if the spatial separation is sufficient to ensure that the first signal to arrive at a receiver is the one assigned to that transmitter. The receiver cards are the heart of the system. Each one incorporates the signal conditioning, peak hold and store, and the counter and latch for one receiver. The address of each receiver card is switch-selectable. The circuits are built on to extended-length single-height eurocards. These cards are mounted in a 19-inch rack with a 64-way backplane. If the system is fully implemented then 21 slots of the available 28 will be filled. A full drawing set is given in Appendix IV.

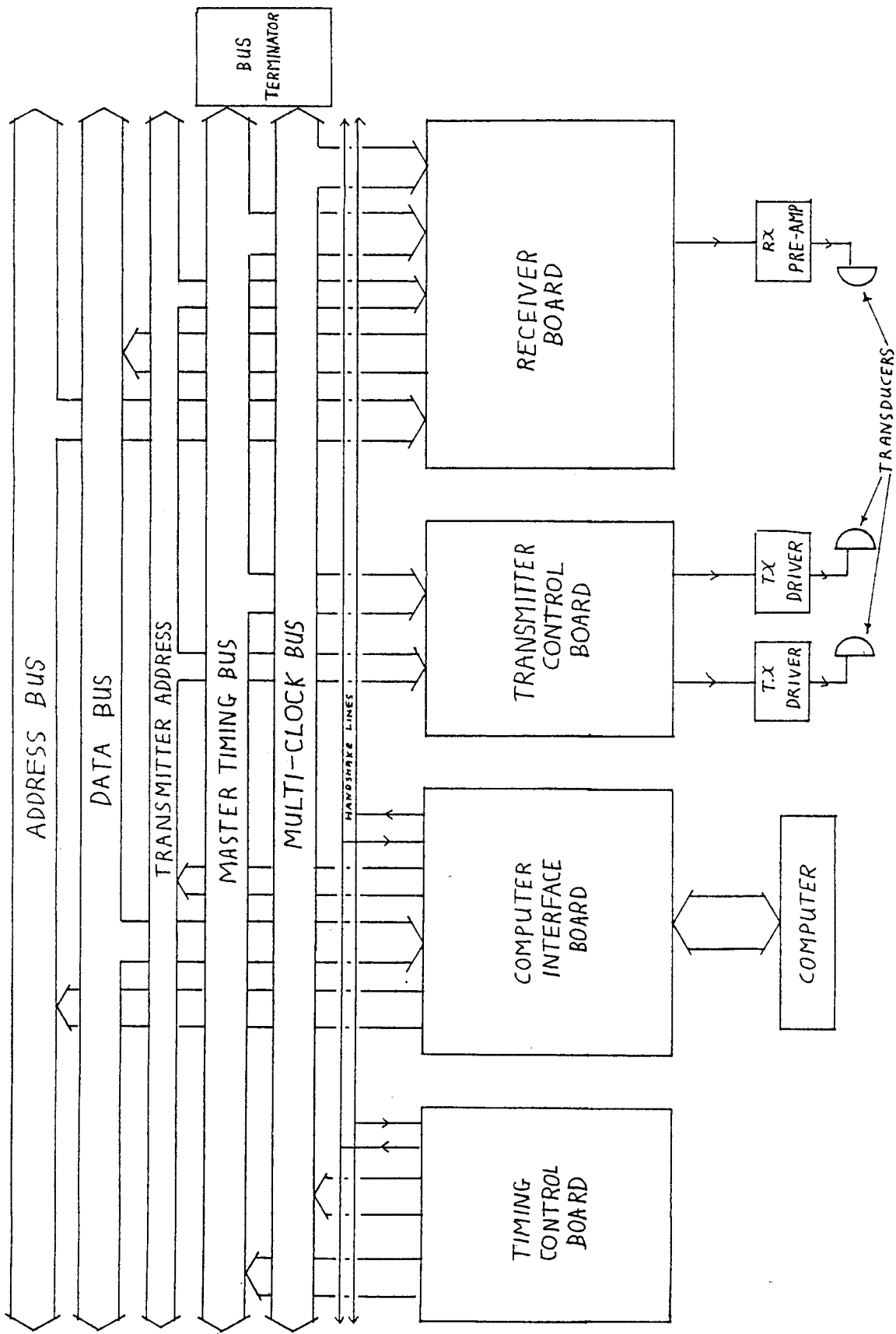


Figure 5.8. Back plane connections of the Eurocard rack.

6) POSITION MEASUREMENT

In order to ascertain the position of a transmitter, a minimum of three receivers are required. More may be used, but this redundancy leads to unnecessary complications. In some circumstances it may be desirable to measure position anywhere in a wide tank. To achieve this an array of receivers can be placed on a tank floor, using the nearest receivers for position calculation. In this case it is simplest to ascertain the position with groups of three receivers, and then average the values obtained with suitable weighting functions. The optimum arrangement of receivers is an equilateral triangle on the tank floor, with the three paths from the transmitter to the receivers forming an orthogonal set. The length of the sides of the triangle will then be $\sqrt{6}$ times the tank depth and the random error in any direction will be the same as for that in determining the distance from transmitter to receiver.

There are three types of error in the position system: fundamental errors caused by mis-evaluation in the speed of sound and the effect of motion of the water through which it passes; electronic error due to random noise and quantisation error; geometric error due to the mis-measurement of the position of the receivers and the mis-evaluation of the delay time through the transmitter and receiver interfaces.

The velocity of sound in water is a function of temperature, static pressure and the presence of soluble additives. Extension data are available for distilled and sea water. The general equation from Kaye and Laby is given below where T is in degrees centigrade, S is salinity in parts per thousand and Z is depth in metres.

$$C = 1449.2 + 4.6 T - 0.055 T^2 + 0.00029 T^3 + (1.34 - 0.01 T)(S - 35) + 0.016 Z$$

Note that this equation was designed to work for salinities of order 35, parts per thousand, so with low salinities errors up to 0.05% may be expected. In a wave tank the effect of depth can be seen to be negligible. The temperature can be measured and its effect compensated for. Salinity is even less of a problem, since in general wave tanks are filled with tap

water which has virtually the same characteristics as distilled water. Our test tank contains additives to prevent corrosion of the metal and biocides to prevent a build-up of fouling. As the main mechanism that varies the speed of sound is density, and as the variation of speed with density is less than 0.1% for every 0.1% change in density, an approximate figure based on the increased density of the water due to the additives should suffice. The temperature of the tank remains at about 16 degrees Celsius throughout the year so the speed of sound has been assumed to be 1478 m/s for this report. As the speed of sound varies by 0.2% per degree, correction for temperature should be used in critical applications.

Even if we assume that the speed of sound relative to the water is constant, the water through which the sound passes is moving and so the speed of sound relative to the receiver does vary. Water movement delays or advances the time the pulse takes to travel from transmitter to receiver, resulting in an error in the measured position. If the transmitter is on the surface vertically above a receiver at depth H , the speed of sound is C and the velocity at depth Z is V , then the transit time T is:-

$$T = \int_0^H \frac{1}{C+V} dz$$

Multiplying by C to give the measured length L and assuming that $C \gg V$ then

$$L-H = \int_0^H \frac{-V}{C} dz$$

This error integral applies also to the surge components of the wave. An error as a percentage of peak wave height is given in Fig 6.1 for a tank of depth 1.2 metres for the errors in both the vertical and horizontal directions. The actual geometry of the transducer arrangement will increase these errors by up to twice these values, so for a wave 10 mm high we can expect a maximum error of 0.04 mm.

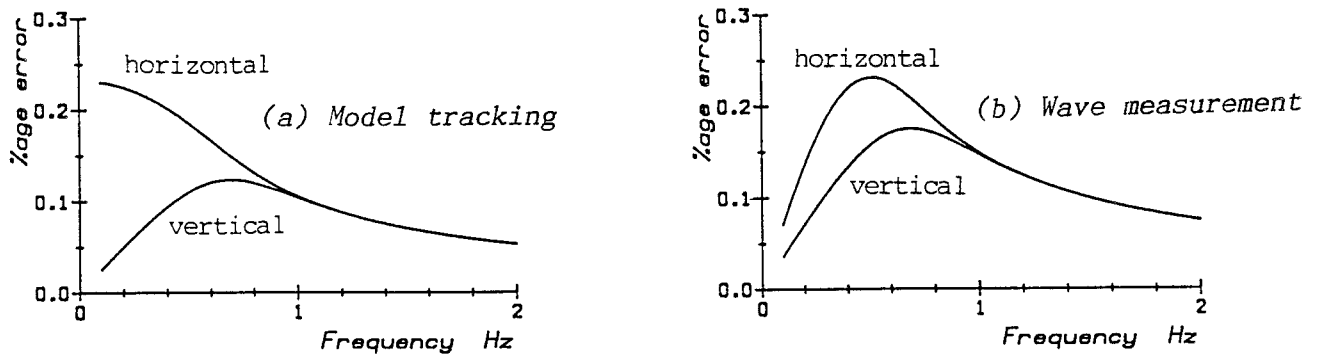


Figure 6.1. Percentage errors caused by the effect of water movement on the sonar signal propagation.

This error is not as significant as it first appears. In wave gauging, the geometry will be well defined and the errors will be only about 1.4 times as great as those shown in Fig 6.1a. Also, at low frequency the motion in surge of the wave action is greater than in heave, so the relative error will be reduced accordingly. A graph of the expected error due to this effect for a 3D wave gauge in a 1.2 metre deep tank is shown in Fig 6.1b. The indicated maximum error of 0.25% is out of phase with the wave motion so it will appear only as a phase advance of less than 0.15 degrees in the sampled wave motion.

For model position measurement such errors may be more significant as the model motion tends to be less than that of the waves. However if the transmitter is positioned only a hundred millimeters below the surface the reduced water velocity in waves 1 Hz and above will give errors less than 0.1%. Model attitude measurements, which require the greatest precision due to the small motion amplitudes, are not corrupted because water velocity affects all of the transmitters equally and the common mode error is rejected.

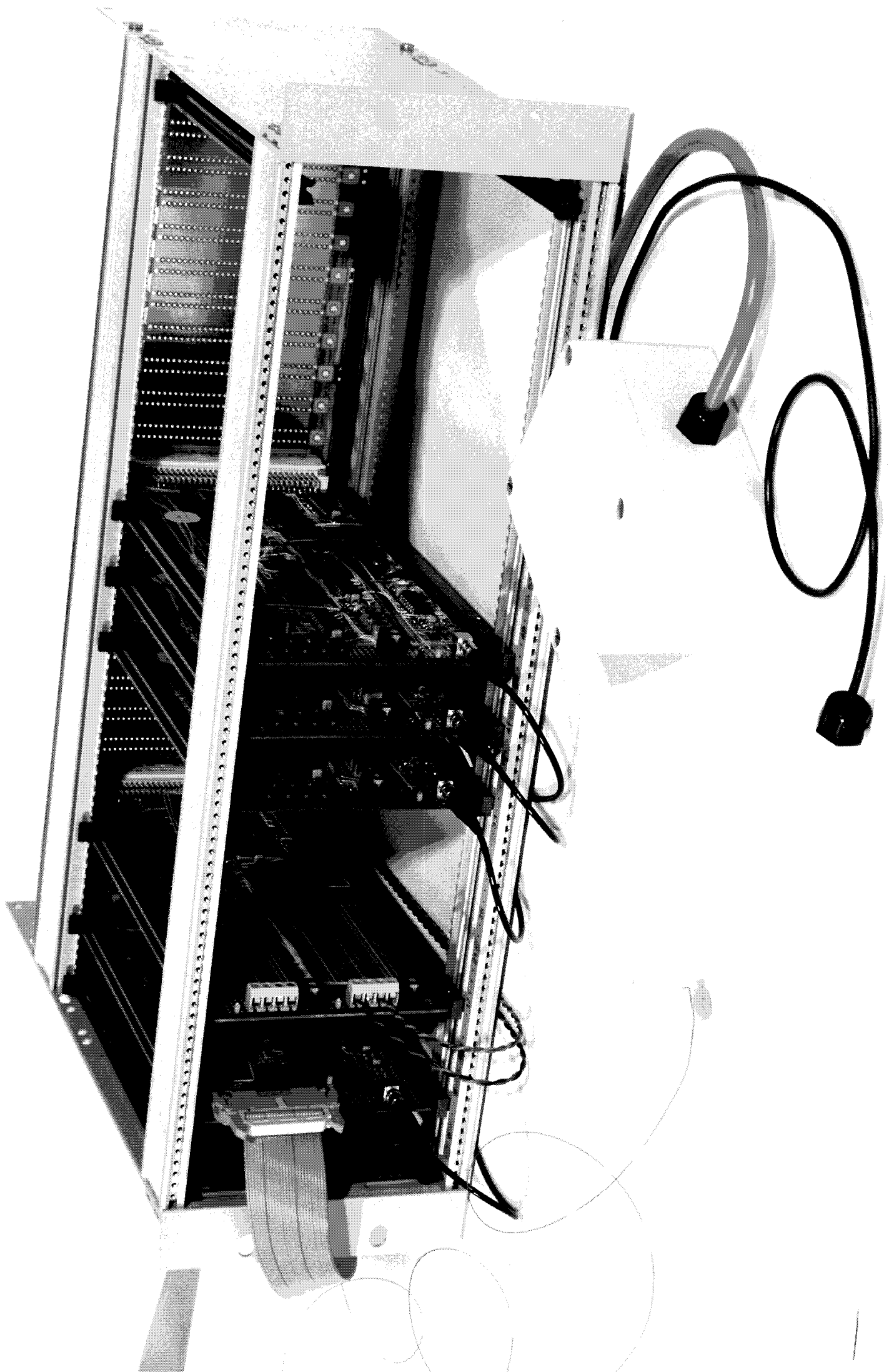
Quantum noise is caused by steps in the output caused by the resolution limit of the electronic counter. This error is particularly serious with small-amplitude regular waves. If the resolution interval can be reduced to the same level as the random noise, then this effect can be ignored. This was achieved in the final version of the electronics.

Errors in receiver position, in the speed of sound and in system delay times cause the geometry used in the mathematical analysis to be in error. This causes cross terms between the three degrees of freedom as well as absolute position errors. It would be possible to overcome this by the use of a

suitable calibration technique but it should be unnecessary to do so as the errors in the position of the receiving sensors should be less than 3 mm. Speed of sound and system delays should not contribute more than 0.1% each. Together these will not give an error of greater than 0.2% of the measured displacement. See the specification section for further details.

It is possible to calculate the position of the transmitter with three receivers provided that the receiver positions are known, that no two receivers are adjacent, and that the transmitter remains on one side of the plane of the receivers. The position is first calculated for a set of axes that contain the three receivers in the XY plane, then rotated to the working plane. For most circumstances the second process will not be necessary if the three receivers are placed at a controlled distance from the bottom of the tank. In calculating the position, the two horizontal displacements can be calculated with only multiplication and addition operations. However, to find the vertical displacement, a square root is necessary. If real-time control is required then a suitable square root algorithm such as Newton-Raphson would be needed. This algorithm will need two iterations starting with the last calculated value as the seed to reduce the error below the quantum error. Each iteration would require a division operation, which is normally slow compared to multiplication and addition. The maximum computation requires 19 additions or subtractions, 21 multiplications and two divisions. Modern digital signal processors can perform this in under 50 microseconds. Control using multiple transmitters and multiple receivers should be easy to implement with sample intervals of a few milliseconds.

The photograph shows the Eurocard rack, the buoy with its ultra light twisted pair connecting lead, one of the three hydrophones and the submerged housing. The system is designed for extension to the tracking of vessels in all six degrees of freedom.



7) WAVEGAUGE EVALUATION

The sonar gauge follows the orbital motion of a water particle on the surface, giving three position variables that relate to the wave field. Many techniques have been developed to extract information about the whole wave field given measurements at particular points. If the waves have been generated by a stochastic process and there are no nearby reflectors, as in the sea, then it is most appropriate to describe the sea state as a distribution in frequency and angle. The maximum likelihood method (Jefferies et al, 1981) can be used to obtain the angular distribution at each frequency if several independent measurements are made. Longuet-Higgins (1963) shows how five parameters, including mean energy flux and direction, describing a directional spectrum can be obtained from the motions of a floating buoy. However, neither approach is appropriate to measurements in wave tanks unless the wave field is forced to appear stochastic by moving the gauge during sampling.

In our tank wave fields are created by the superposition of wave fronts and the method of analysis should resolve the waves with a similar description. Since there are some combinations of waves which produce the same orbital motion at a particular place, this approach must be followed with care or with some prior assumptions.

Two wave assumption

Suppose the wave field can be represented by two plane waves with complex amplitudes a , b and angles of incidence α , β . The resulting orbital amplitudes in shallow water are then

$$x = \frac{i}{\tanh(kh)} (a \cos \alpha + b \cos \beta) \quad (7.1)$$

$$y = \frac{i}{\tanh(kh)} (a \sin \alpha + b \sin \beta) \quad (7.2)$$

$$z = a + b \quad (7.3)$$

These equations are completely soluble for a, b, α, β and the solution is described in Appendix III. Note that there are a number of circumstances under which the parameters cannot be found.

Two-component wave field

To illustrate the circumstances in which resolution of the wave field into two components succeeds and fails, two incident waves were specified with equal magnitude and direction $\pi/6$ and $-\pi/6$ respectively. The phase of the second wave was varied through a complete cycle in a series of tests.

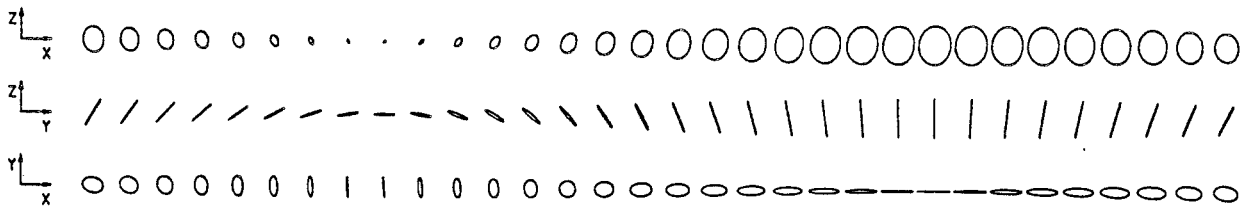


Figure 7.1. The three orbital motions of a two component wave field.

Fig 7.1 shows the orbital motion of the wave gauge viewed along each of the three axes. The same orbital motions could have been obtained by traversing the gauge across the wave field instead of altering the second wave phase.

Fig 7.2 shows the magnitudes of the orbital amplitudes and the parameters for the two waves which can be calculated from these. There are two sizeable regions where the method fails. When the x and z motions are small the motion is in y only and could have been generated by varying the angle and magnitude of the wave pair. Problems also occur when there is x and z motion only since the same orbital motion could have been caused by an incident wave at angle 0 and a reflected wave at π . In the intermediate regions the method resolves the waves well.

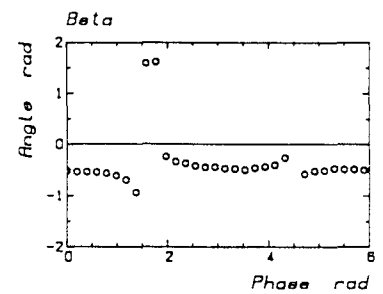
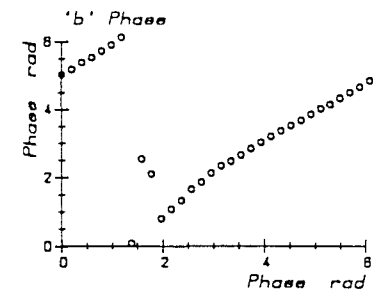
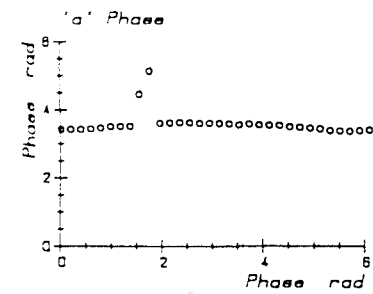
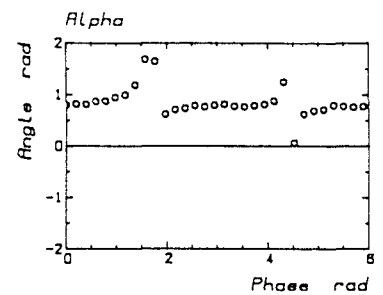
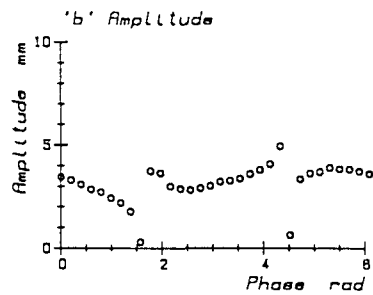
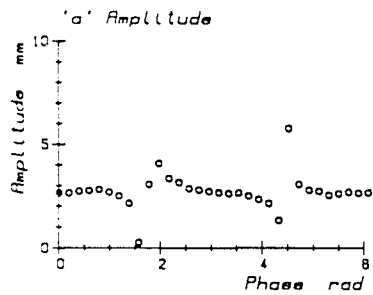
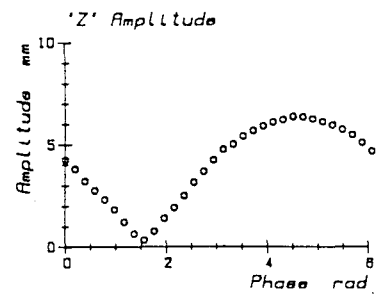
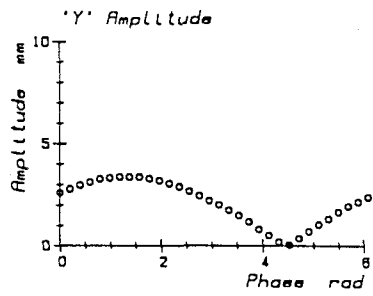
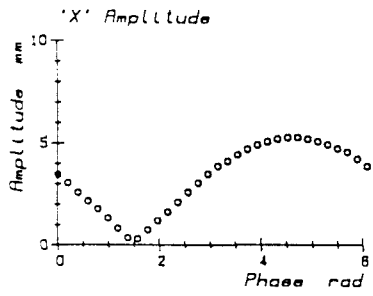


Figure 7.2. X Y and Z components and their resolution into the original wave fronts. Not all phase combinations give satisfactory results.

Resolution of angled waves

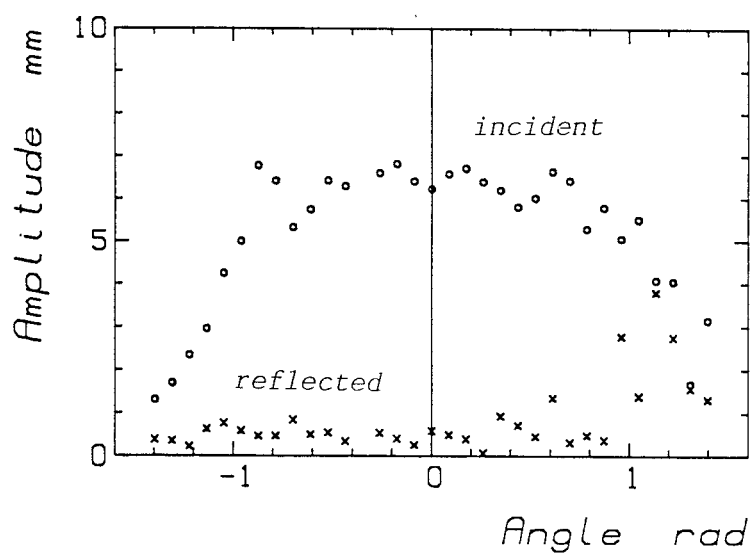
In model wave tanks most wave fields are generated with only one component at each frequency. This ensures that the incident flux is spatially homogeneous with no energy 'hot spots'. However, reflections from the beaches and tank walls interfere with the incident waves and a particularly important use of a 3D wave gauge is the resolution of angled incident waves from small reflections.

Fig 7.3 shows the results of an experiment with angled waves in range $-\pi/2$ to $+\pi/2$. For all angled waves there is a region of the tank where the water is relatively calm and it can be seen that the wave gauge was in this area for angles beyond ± 0.8 radian. We would normally only test with waves between these bounds.

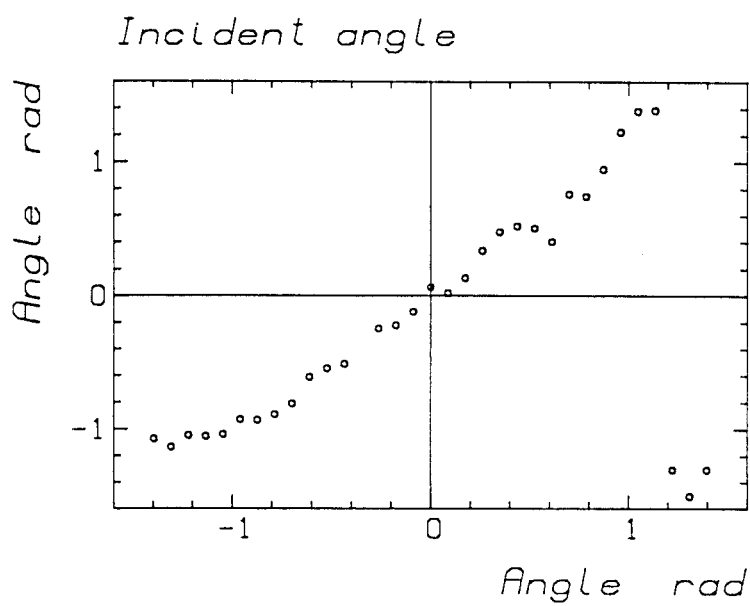
Within the working region the measured angle is within .1 radian (5 deg) of that specified, and the amplitude varies by $\pm 5\%$. These errors are greater than the assumed capabilities of our tank, and suggest additional errors due to reflected waves and imperfect wave following of the buoy.

Outside the central area the incident wave amplitude drops off from the specified value. For large positive angles the glass side-wall of the tank acts as a reflector causing confusion in the resolution of the wave components. For large negative angles the measured angle is less than that requested because of the diffraction of the wave field into the calm region.

The wave gauge performed well under these conditions and could be used with spectra with only one generated component at each frequency. However, the analysis would have failed if any of the unresolvable cases had been encountered. By assuming the relative magnitudes of the waves, or their approximate angles ambiguities might be reduced.



(a)



(b)

Figure 7.3. Angle measurement.

Resolution of incident and reflected waves

In Fig 7.4 the incident and reflected wave amplitudes plotted for the sonar gauge (symbols) analysed by two methods, and similar measurements made with an array of wave probes (continuous line). The experiments consisted of a series of tests in which regular waves of nominal amplitude 4mm and angle 0 were generated at a range of frequencies from 0.4 Hz to 1.6 Hz.

The experiment with the array of wave gauges was conducted one metre to the side of the sonar gauge and about two months earlier, so is not strictly comparable. The array consisted of 24 equally spaced wave probes in a line 3 metres long, and from the collected wave records incident and reflected wave amplitudes were identified. The results are smoother because of averaging along the array.

In Fig 7.4a the symbols show the results of the analysis from the sonar gauge using the two wave resolution described already. The results compare well with those from the array, but there are several anomalies where the wave field is confused with other possibilities.

If it is assumed that the reflected wave is small compared with the incident, equations (7.1), (7.2), (7.3) can be 'solved' in a different way. Setting $\mathbf{b} = 0$ and dividing (7.2) by (7.1) yields

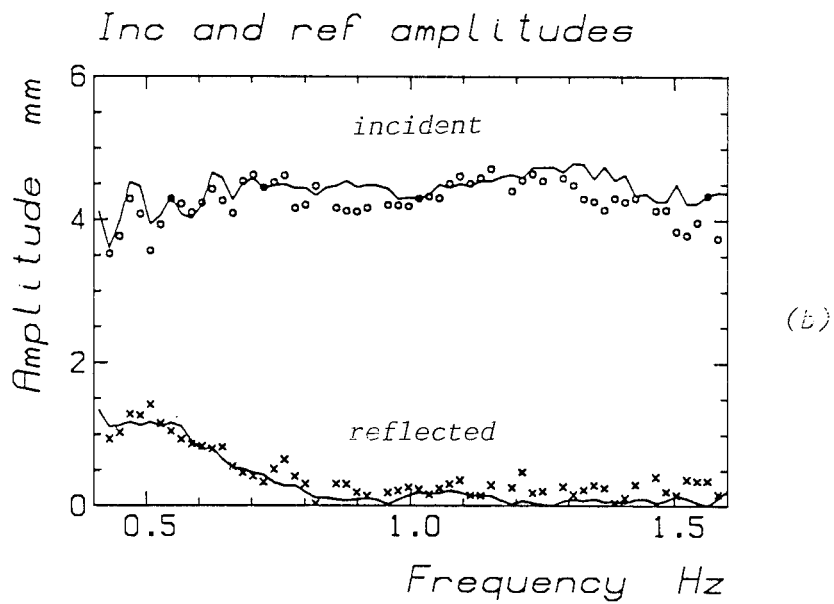
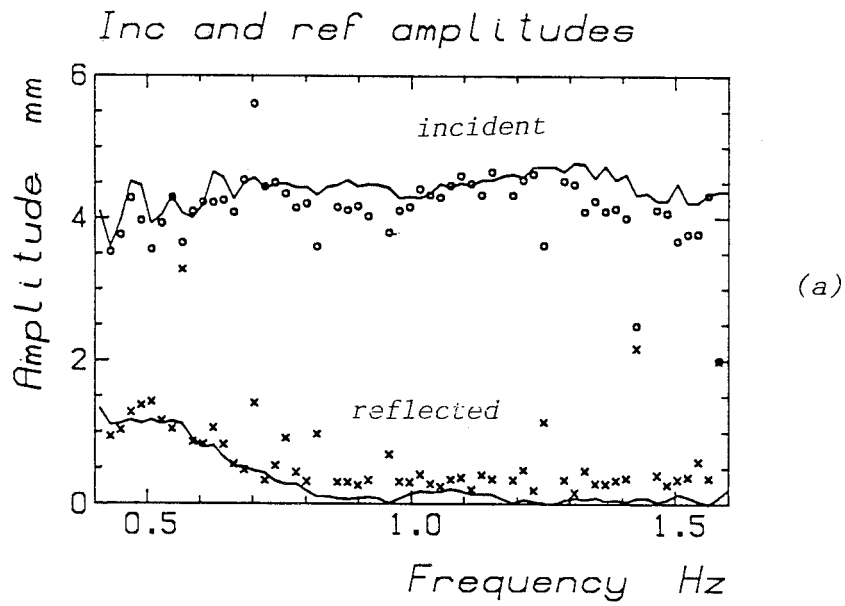
$$\tan \alpha = \operatorname{Re}\{y/x\}$$

Which is sufficiently accurate to provide a good estimate for $\cos \alpha$. Assuming β is close to π , \mathbf{b} can be eliminated by adding (7.1) and (7.3)

$$\mathbf{a} = (z - i x \tanh(kh)) / (1 + \cos \alpha)$$

And \mathbf{b} is found by substituting back into (7.3)

The results found by analysing the measurements in this way are plotted in Fig 7.4b. The incident amplitude falls away from that measured by the wave gauge array at higher frequencies as the buoy's size becomes comparable to the wavelength. The small amplitude of the measured reflection is a good indication of the ability of the buoy to follow the water orbitals.



Resolving the incident and reflected wave using a 3-D wavegauge

Fig 5.4

Spectra

To determine the performance of the wavegauge in a mixed wave field we measured with seas repeat times of 12.5 seconds and various angular spreads. The seas conformed to the Pierson Moskowitz frequency spectrum with an average period of 1 second. We used \cos^n spreadings with n between 1 and 64. The results are plotted in Fig 7.5. The **Z** axis is vertical with **X** in the mean direction of the waves and **Y** at right angles to it. These plots clearly show the effect of increasing the spreading function on the amplitude of the wave in the **Y** dimension. It is also noticeable that the wave in the **X** dimension equals that in the **Z** dimension at high spreadings, but not at low spreadings.

While no attempt has been made to analyse the results from mixed seas, the results so far obtained indicate that this gauge could be a valuable tool in assessing wave fields in tanks used for random testing. It is our belief that such work would be improved if there was a facility to move the position of the buoy during the sampling period, allowing statistical techniques such as maximum likelihood method to be used.

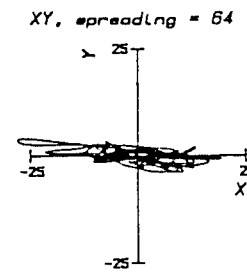
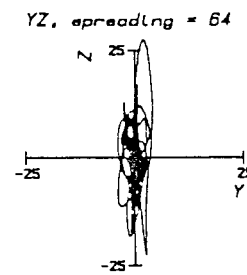
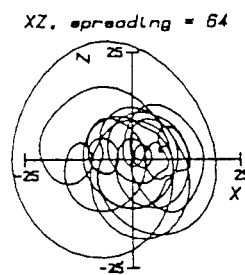
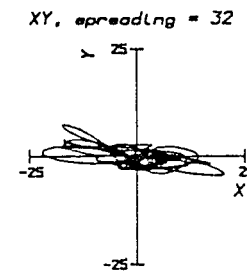
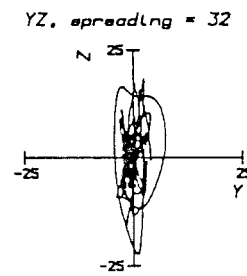
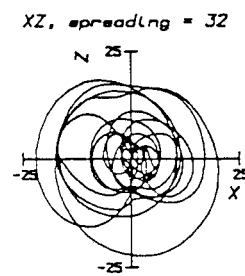
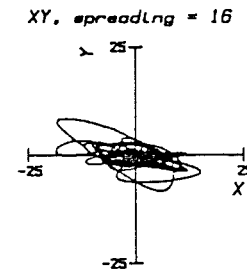
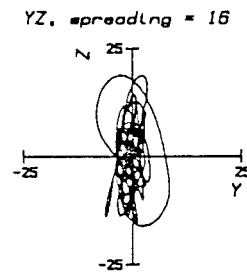
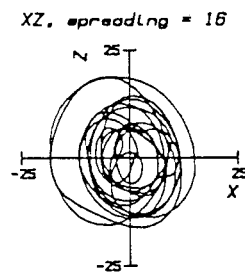
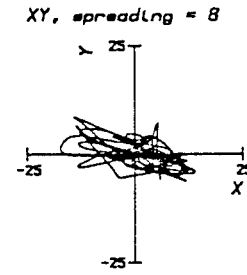
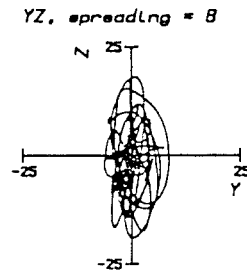
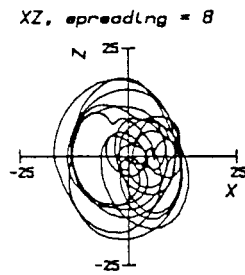
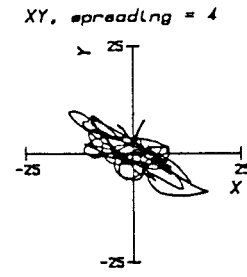
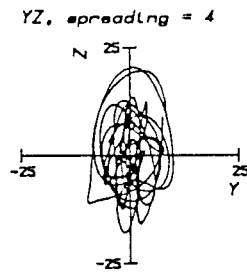
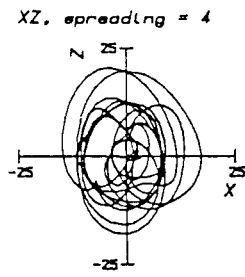
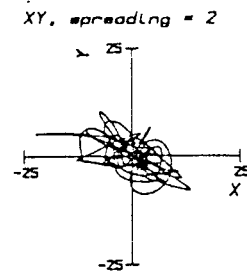
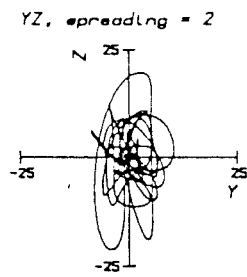
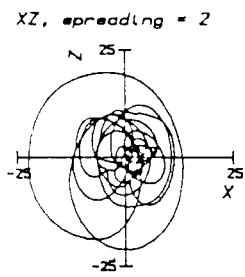


Figure 7.5. Lissajous plots of Pierson Moskowitz spectra with various spreading functions as seen along each axis.

8) SPECIFICATION OF SONAR MEASUREMENT SYSTEM

In all configurations there can be a maximum of 16 receivers and 4 independent transmitters. Piezo electric transducers are 12.7 mm diameter hemispheres or spheres throughout. Receivers and transmitters shall be within 3 metres of their conditioning circuits. The receiver preamplifier can be up to 40 metres from the rack mounted electronics, while the transmitter driver can be up to 100 metres away.

Wavegauging

Wavegauging using a 50 mm diameter buoy with three, double float/sinker moorings constructed of 0.7 gm weights and 0.5 Kg breaking strain fishing line. Signal to the transmitting piezo electric device carried through a twisted pair of 0.06 mm diameter enamelled copper wire.

Resolution	20	m	
Accuracy	$\pm 1.5\%$	± 30	m Up to 1.4 Hz
	$\pm 10\%$	± 30	m Up to 2.5 Hz

Position measurement of vessels

For a position measurement system consisting of one transmitter and three receivers 1 to 1.5 metres below the water surface, and approximately 3 metres apart. The transmitter is to be submerged 100 mm below the water surface. Waves of frequency 0.5 Hz and upwards may be present.

Resolution	20 m	
Accuracy	$\pm 0.1\% \pm 30$ m	No waves
	$\pm 0.1\% \pm 50$ m	Waves up to 10 mm high
	$\pm 0.1\% \pm 80$ m	Waves up to 50 mm high

Attitude measurement of vessels

As for position measurement except for the use of transmitters in pairs. Each pair to be at least 100 mm apart and at least 100 mm below the surface. Increased spacing will improve specification linearly.

Resolution	200 μ R or 0.7 Arc minutes	
Accuracy	$\pm 500 \mu$ R or ± 2 Arc minutes	Waves up to 100 mm high

APPENDICES

I) POSITION CALCULATION

The sonar system measures the distance from the transmitter to each of three receivers on the tank floor. The position of the transmitter can be determined from these lengths and the positions of the receivers. If the receivers all lie in the same z-plane the calculation is greatly simplified and this case is described first, followed by the rotation needed to transform any reference frame into this special frame.

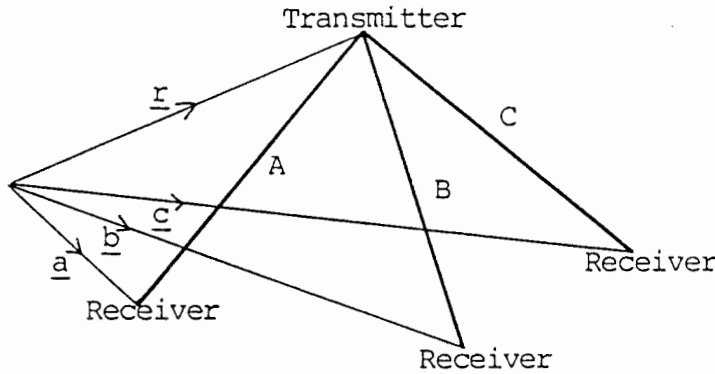


Fig I.1

Figure (I.1) shows the sonar transmitter along with three sonar receivers. The receivers have known position vectors

$$\underline{a} = (a_x, a_y, a_z),$$

$$\underline{b} = (b_x, b_y, b_z),$$

$$\underline{c} = (c_x, c_y, c_z)$$

The transmitter has an unknown position vector $\underline{r} = (x, y, z)$

which can be calculated from the three measured lengths A, B and C

$$|\underline{r} - \underline{a}| = A \quad (\text{I.1})$$

$$|\underline{r} - \underline{b}| = B \quad (\text{I.2})$$

$$|\underline{r} - \underline{c}| = C \quad (\text{I.3})$$

Squaring yields

$$|\underline{r}|^2 - 2 \underline{r} \cdot \underline{a} + |\underline{a}|^2 = A^2 \quad (\text{I.4})$$

$$|\underline{r}|^2 - 2 \underline{r} \cdot \underline{b} + |\underline{b}|^2 = B^2 \quad (\text{I.5})$$

$$|\underline{r}|^2 - 2 \underline{r} \cdot \underline{c} + |\underline{c}|^2 = C^2 \quad (\text{I.6})$$

Expanding the scalar product

$$|\underline{r}|^2 - 2(x a_x + y a_y + z a_z) + |\underline{a}|^2 = A^2 \quad (\text{I.7})$$

$$|\underline{r}|^2 - 2(x b_x + y b_y + z b_z) + |\underline{b}|^2 = B^2 \quad (\text{I.8})$$

$$|\underline{r}|^2 - 2(x c_x + y c_y + z c_z) + |\underline{c}|^2 = C^2 \quad (\text{I.9})$$

Multiplying (I.7), (I.8), (I.9) by $(b_y - c_y)$, $(c_y - a_y)$, $(a_y - b_y)$ respectively and summing to eliminate $|r|^2$ and y

$$\begin{aligned} (x a_x + z a_z) (b_y - c_y) &= (A^2 - |\underline{a}|^2) (b_y - c_y) \\ + (x b_x + z b_z) (c_y - a_y) &+ (B^2 - |\underline{b}|^2) (c_y - a_y) \\ + (x c_x + z c_z) (a_y - b_y) &+ (C^2 - |\underline{c}|^2) (a_y - b_y) \end{aligned} \quad (\text{I.10})$$

If the receivers all have the same z coordinate ($a_z = b_z = c_z$) equation (I.10) simplifies leaving

$$x = \frac{A^2 (b_y - c_y) + B^2 (c_y - a_y) + C^2 (a_y - b_y) - [|\underline{a}|^2 (b_y - c_y) + |\underline{b}|^2 (c_y - a_y) + |\underline{c}|^2 (a_y - b_y)]}{2 [a_x (b_y - c_y) + b_x (c_y - a_y) + c_x (a_y - b_y)]}$$

(I.11)

Since equations (I.7) -> (I.9) are symmetrical in x and y

$$y = \frac{A^2 (b_x - c_x) + B^2 (c_x - a_x) + C^2 (a_x - b_x) - [|\underline{a}|^2 (b_x - c_x) + |\underline{b}|^2 (c_x - a_x) + |\underline{c}|^2 (a_x - b_x)]}{2 [a_y (b_x - c_x) + b_y (c_x - a_x) + c_y (a_x - b_x)]}$$

(I.12)

Expanding equation (I.7)

$$x^2 + y^2 + z^2 - 2(x a_x + y a_y + z a_z) + |\underline{a}|^2 = A^2$$

Hence

$$z = a_z + \sqrt{A^2 - a_x^2 - a_y^2 - x^2 - y^2 - 2x a_x - 2y a_y}$$

(I.13)

Equations (I.11), (I.12), (I.13) can be used to calculate x, y, z from the lengths A, B, C . Most of the terms are constant expressions which could be precalculated so that the position might be determined in real time with only a few operations.

$$x = K_1 A^2 + K_2 B^2 + K_3 C^2 + K_4 \quad (\text{I.14})$$

$$y = K_5 A^2 + K_6 B^2 + K_7 C^2 + K_8 \quad (\text{I.15})$$

$$z = K_9 + \sqrt{A^2 + K_{10} - x^2 - y^2 + K_{11}x + K_{12}y} \quad (\text{I.16})$$

With K_j found from (I.11), (I.12), (I.13)

Position calculation for general geometry

If the reference frame S does not contain the receivers in the same z -plane a new frame S' can always be found which does.

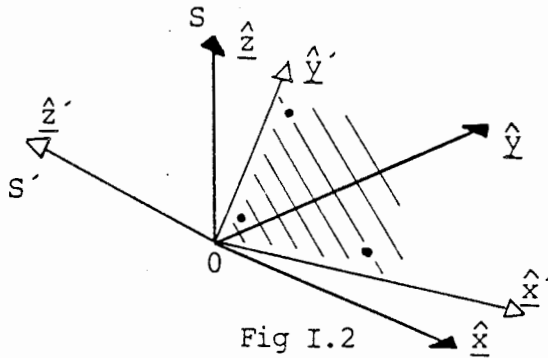


Fig I.2

Fig I.2 shows the two coordinate systems with axes \hat{x} , \hat{y} , \hat{z} and \hat{x}' , \hat{y}' , \hat{z}' . The vector \hat{z}' must be perpendicular to the plane of the receivers and can be formed from the vector product of two of the sides of the base

$$\hat{z}' = \frac{(\underline{a} - \underline{b}) \wedge (\underline{b} - \underline{c})}{|(\underline{a} - \underline{b}) \wedge (\underline{b} - \underline{c})|} \quad (\text{I.17})$$

\hat{x}' must be perpendicular to \hat{z}' . Choose

$$\underline{x}' = \frac{(\hat{z}'_z, 0, \hat{z}'_x)}{\sqrt{z_z'^2 + z_x'^2}} \quad (\text{I.18})$$

\hat{y}' is formed from the vector product of \hat{z}' and \hat{x}'

$$\hat{y}' = \hat{z}' \wedge \hat{x}' \quad (\text{I.19})$$

Vectors can be rotated into the frame S' by the transformation

$$\underline{v}' = \underline{\underline{L}} \cdot \underline{v} \quad (\text{I.20})$$

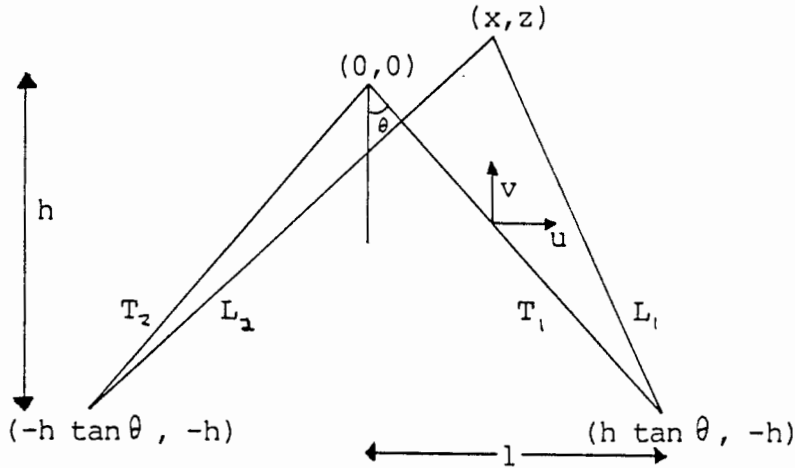
$$\text{where } \underline{\underline{L}} = \begin{bmatrix} \hat{x}'_x & \hat{x}'_y & \hat{x}'_z \\ \hat{y}'_x & \hat{y}'_y & \hat{y}'_z \\ \hat{z}'_x & \hat{z}'_y & \hat{z}'_z \end{bmatrix} \quad (\text{I.21})$$

And rotated back by

$$\underline{v} = \underline{\underline{L}}^T \cdot \underline{v}' \quad (\text{I.22})$$

If the receivers do not lie in the same z -plane, the transformation matrix (I.21) should be found, the position vectors \underline{a} , \underline{b} , \underline{c} rotated with it, the vector \underline{r}' found using (I.11), (I.12), (I.13), then the vector \underline{r} in S found from (I.22).

II) ERRORS DUE TO WAVE MOTION



Consider a transmitter on the surface of the water at the origin and two receivers placed symmetrically on the tank floor. The transit time for a sonar pulse between transmitter and receiver is effected by the components of the water particle velocity, and the velocity field is assumed to vary vertically but not horizontally. The transit time is

$$T = \int_0^{-h} \frac{l}{(-c - u \sin\theta + v \cos\theta) \cos\theta} dz \quad (II.1)$$

If u and v are small compared to c , (II.1) can be approximated to

$$T = \int_0^{-h} \frac{-l}{c \cos\theta} (1 - \frac{u}{c} \sin\theta + \frac{v}{c} \cos\theta) dz \quad (II.2)$$

For a wave with amplitude A_0 the water particles with vertical and horizontal motions A_v and A_u

$$A_v = A_0 \sin \omega t \frac{\sinh(k(h+z))}{\sinh(kh)} \quad (II.3)$$

$$A_u = A_0 \cos \omega t \frac{\cosh(k(h+z))}{\sinh(kh)} \quad (II.4)$$

Where k is defined by

$$\omega^2 = gk \tanh(kh) \quad (II.5)$$

The vertical and horizontal water velocities are

$$v = A_0 \omega \cos \omega t \frac{\sinh(k(h+z))}{\sinh(kh)} \quad (II.6)$$

$$u = -A_0 \omega \sin \omega t \frac{\cosh(k(h+z))}{\sinh(kh)} \quad (II.7)$$

Substituting for v, u from (II.6), (II.7) into (II.2)

$$T_1 = \frac{h}{c \cos \theta} + \frac{A_0 \omega \tan \theta}{c} \sin \omega t \int_0^{-h} \frac{\cosh(k(h+z))}{\sinh(kh)} dz + \frac{A_0 \omega \cos \omega t}{c} \int_0^{-h} \frac{\sinh(k(h+z))}{\sinh(kh)} dz \quad (\text{II.8})$$

Integrating yields

$$T_1 = \frac{h}{c \cos \theta} + \frac{A_0 \omega \tan \theta}{c^2 k} \sin \omega t \left[\frac{\sinh(k(h+z))}{\sinh(kh)} \right]_0^{-h} + \frac{A_0 \omega \cos \omega t}{c^2 k} \left[\frac{\cosh(k(h+z))}{\sinh(kh)} \right]_0^{-h} \quad (\text{II.9})$$

$$T_1 = \frac{h}{c \cos \theta} - \frac{A_0 \omega \tan \theta}{c^2 k} \sin \omega t - \frac{A_0 \omega (\cosh(kh) - 1)}{c^2 k \sinh(kh)} \quad (\text{II.10})$$

If the unmodified speed of sound was used to calculate L_1 , L_2 then

$$L_1 = \frac{h}{\cos \theta} - A_0 \sin \omega t \frac{\omega}{ck} \tan \theta - A_0 \cos \omega t \frac{\omega}{ck} \frac{(\cosh(kh) - 1)}{\sinh(kh)} \quad (\text{II.11})$$

$$L_2 = \frac{h}{\cos \theta} + A_0 \sin \omega t \frac{\omega}{ck} \tan \theta - A_0 \cos \omega t \frac{\omega}{ck} \frac{(\cosh(kh) - 1)}{\sinh(kh)} \quad (\text{II.12})$$

For convenience define

$$E_1 = A_0 \cos \omega t \frac{\omega}{ck} \frac{(\cosh(kh) - 1)}{\sinh(kh)} \quad (\text{II.13})$$

$$E_2 = A_0 \sin \omega t \frac{\omega}{ck} \quad (\text{II.14})$$

Substituting into (II.11), (II.12)

$$L_1 = \frac{h}{\cos \theta} - E_2 \tan \theta - E_1 \quad (\text{II.15})$$

$$L_2 = \frac{h}{\cos \theta} + E_2 \tan \theta - E_1 \quad (\text{II.16})$$

These lengths calculated from the receiver measurements give a false position vector (x, z). Since the receivers have position vectors (h tan θ, -h) and (-h tan θ, -h) respectively

$$(x - h \tan \theta)^2 + (z + h)^2 = L_1^2 \quad (\text{II.17})$$

$$(x + h \tan \theta)^2 + (z + h)^2 = L_2^2 \quad (\text{II.18})$$

Subtracting (II.17) from (II.18) gives

$$-4xh \tan \theta = L_2^2 - L_1^2 \quad (\text{II.19})$$

Substituting for L_1, L_2 from (II.15), (II.16)

$$-4xh \tan \theta = -4 \frac{h}{\cos \theta} E_2 \tan \theta + 4 E_1 E_2 \tan \theta \quad (\text{II.20})$$

If $E \ll h$ the second order term can be ignored and

$$x = \frac{E_2}{\cos \theta} \quad (\text{II.21})$$

Adding (II.17) and (II.18) yields

$$2x^2 + 2(h \tan \theta)^2 + 2z^2 + 4zh + 2h^2 = L_1^2 + L_2^2 \quad (\text{II.22})$$

Substituting for L_1, L_2 from (II.15), (II.16)

$$2x^2 + 2(h \tan \theta)^2 + 2z^2 + 4zh + 2h^2 = 2 \left(\frac{h}{\cos \theta} \right)^2 + 2(E_2 \tan \theta)^2 + 2E_1^2 - 4E_1 \frac{h}{\cos \theta} \quad (\text{II.23})$$

But by Pythagoras

$$h^2 + (h \tan \theta)^2 = \left(\frac{h}{\cos \theta} \right)^2 \quad (\text{II.24})$$

Using this identity and ignoring second order terms in E_1, E_2 (II.23) becomes

$$2x^2 + 2z^2 + 4zh = -4E_1 \frac{h}{\cos \theta} \quad (\text{II.25})$$

If $x \ll h$ and $z \ll h$ (II.25) can be approximated

$$z = \frac{E_1}{\cos \theta} \quad (\text{II.26})$$

Substituting for E_1, E_2 from (II.13), (II.14) into (II.21), (II.26) gives the errors in surge and heave due to the effect of the water motion on the velocity of sound

$x = A \sin(\omega t) \frac{\omega}{ck} \frac{1}{\cos \theta} \quad (\text{II.27})$

$z = A \cos(\omega t) \frac{\omega}{ck} \frac{(\cosh(kh) - 1)}{\sinh(kh)} \frac{1}{\cos \theta} \quad (\text{II.28})$

III) RESOLUTION OF TWO PLANE WAVES FOR A SINGLE WAVEGAUGE

The wave field is assumed to consist of two plane waves with complex amplitudes a , b and angles of incidence α , β . The equations for x , y , z given in section (5) and can be solved for these parameters.

$$x = \frac{i}{\tanh(kh)} (a \cos\alpha + b \cos\beta) \quad [7.1]$$

$$y = \frac{i}{\tanh(kh)} (a \sin\alpha + b \sin\beta) \quad [7.2]$$

$$z = a + b \quad [7.3]$$

Define new variables X , Y , Z for ease of manipulation

$$X = \frac{\tanh(kh)}{i} x \quad (\text{III.1})$$

$$Y = \frac{\tanh(kh)}{i} y \quad (\text{III.2})$$

$$Z = z \quad (\text{III.3})$$

Then

$$X = a \cos\alpha + b \cos\beta \quad (\text{III.4})$$

$$Y = a \sin\alpha + b \sin\beta \quad (\text{III.5})$$

$$Z = a + b \quad (\text{III.6})$$

Solving (III.4), (III.5) for a , b

$$a = \frac{\begin{vmatrix} X & \cos\beta \\ Y & \cos\beta \end{vmatrix}}{\begin{vmatrix} \cos\alpha & \cos\beta \\ \sin\alpha & \sin\beta \end{vmatrix}} = \frac{X \sin\beta - Y \cos\beta}{\sin(\beta - \alpha)} \quad (\text{III.7})$$

$$b = \frac{\begin{vmatrix} \cos\alpha & X \\ \cos\alpha & Y \end{vmatrix}}{\begin{vmatrix} \cos\alpha & \cos\beta \\ \sin\alpha & \sin\beta \end{vmatrix}} = \frac{-X \sin\alpha + Y \cos\alpha}{\sin(\beta - \alpha)} \quad (\text{III.8})$$

Substituting into (III.6) and dividing into real and imaginary parts

$$\text{Re}\{Z\} \sin(\beta - \alpha) = \text{Re}\{X\} (\sin\beta - \sin\alpha) + \text{Re}\{Y\} (\cos\beta - \cos\alpha) \quad (\text{III.9})$$

$$\text{Im}\{Z\} \sin(\beta - \alpha) = \text{Im}\{X\} (\sin\beta - \sin\alpha) + \text{Im}\{Y\} (\cos\beta - \cos\alpha) \quad (\text{III.10})$$

Hence

$$\sin \beta - \sin \alpha = \frac{\begin{vmatrix} \operatorname{Re}\{Z\} & \operatorname{Re}\{Y\} \\ \operatorname{Im}\{Z\} & \operatorname{Im}\{Y\} \end{vmatrix}}{\begin{vmatrix} \operatorname{Re}\{X\} & \operatorname{Re}\{Y\} \\ \operatorname{Im}\{X\} & \operatorname{Im}\{Y\} \end{vmatrix}} \sin(\beta - \alpha) = \Delta_1 \sin(\beta - \alpha) \quad (\text{III.11})$$

And

$$\cos \beta - \cos \alpha = \frac{\begin{vmatrix} \operatorname{Re}\{X\} & \operatorname{Re}\{Z\} \\ \operatorname{Im}\{X\} & \operatorname{Im}\{Z\} \end{vmatrix}}{\begin{vmatrix} \operatorname{Re}\{X\} & \operatorname{Re}\{Y\} \\ \operatorname{Im}\{X\} & \operatorname{Im}\{Y\} \end{vmatrix}} \sin(\beta - \alpha) = \Delta_2 \cos(\beta - \alpha) \quad (\text{III.12})$$

Where

$$\Delta_1 = \frac{\begin{vmatrix} \operatorname{Re}\{Z\} & \operatorname{Re}\{Y\} \\ \operatorname{Im}\{Z\} & \operatorname{Im}\{Y\} \end{vmatrix}}{\begin{vmatrix} \operatorname{Re}\{X\} & \operatorname{Re}\{Y\} \\ \operatorname{Im}\{X\} & \operatorname{Im}\{Y\} \end{vmatrix}} \quad (\text{III.13})$$

$$\Delta_2 = \frac{\begin{vmatrix} \operatorname{Re}\{X\} & \operatorname{Re}\{Z\} \\ \operatorname{Im}\{X\} & \operatorname{Im}\{Z\} \end{vmatrix}}{\begin{vmatrix} \operatorname{Re}\{X\} & \operatorname{Re}\{Y\} \\ \operatorname{Im}\{X\} & \operatorname{Im}\{Y\} \end{vmatrix}} \quad (\text{III.14})$$

Using standard trigonometric relations (III.11), (III.12) become

$$\begin{aligned} 2 \cos \frac{1}{2}(\beta + \alpha) \sin \frac{1}{2}(\beta - \alpha) &= \Delta_1 2 \cos \frac{1}{2}(\beta - \alpha) \sin \frac{1}{2}(\beta - \alpha) \\ \rightarrow \cos \frac{1}{2}(\beta + \alpha) &= \Delta_1 \cos \frac{1}{2}(\beta - \alpha) \end{aligned} \quad (\text{III.15})$$

$$\begin{aligned} 2 \sin \frac{1}{2}(\beta + \alpha) \sin \frac{1}{2}(\beta - \alpha) &= \Delta_2 2 \cos \frac{1}{2}(\beta - \alpha) \sin \frac{1}{2}(\beta - \alpha) \\ \rightarrow \sin \frac{1}{2}(\beta + \alpha) &= \Delta_2 \cos \frac{1}{2}(\beta - \alpha) \end{aligned} \quad (\text{III.16})$$

Squaring and adding (III.15), (III.16)

$$\begin{aligned} 1 &= (\Delta_1^2 + \Delta_2^2) \cos^2 \frac{1}{2}(\beta - \alpha) \\ \rightarrow \cos(\beta - \alpha) &= \frac{2}{\Delta_1^2 + \Delta_2^2} - 1 \end{aligned} \quad (\text{III.17})$$

Squaring and adding (III.4), (III.5) yields an equation containing $\cos(\beta - \alpha)$

$$X^2 + Y^2 = a^2 + b^2 + 2ab \cos(\beta - \alpha) \quad (\text{III.18})$$

Squaring (III.6)

$$Z^2 = a^2 + b^2 + 2ab \quad (\text{III.19})$$

Subtracting (III.18), (III.19)

$$X^2 + Y^2 - Z^2 = 2ab (\cos(\beta - \alpha) - 1) \quad (\text{III.20})$$

Substituting for b from (III.6)

$$X^2 + Y^2 - Z^2 = 2a(Z-a) (\cos(\beta - \alpha) - 1)$$

$$\rightarrow a^2 - Za + \frac{X^2 + Y^2 - Z^2}{2(\cos(\beta - \alpha) - 1)} = 0 \quad (\text{III.21})$$

Equation (III.22) has two solutions which because of the symmetry of a and b correspond to each

$$a = \frac{Z}{2} + \frac{1}{2} \sqrt{Z^2 - \frac{2(X^2 + Y^2 - Z^2)}{(\cos(\beta - \alpha) - 1)}} \quad (\text{III.22})$$

$$b = \frac{Z}{2} - \frac{1}{2} \sqrt{Z^2 - \frac{2(X^2 + Y^2 - Z^2)}{(\cos(\beta - \alpha) - 1)}} \quad (\text{III.23})$$

By separating each of equations (III.4), (III.5) into real and imaginary parts $\cos\alpha$, $\cos\beta$ and $\sin\alpha$, $\sin\beta$ can be found

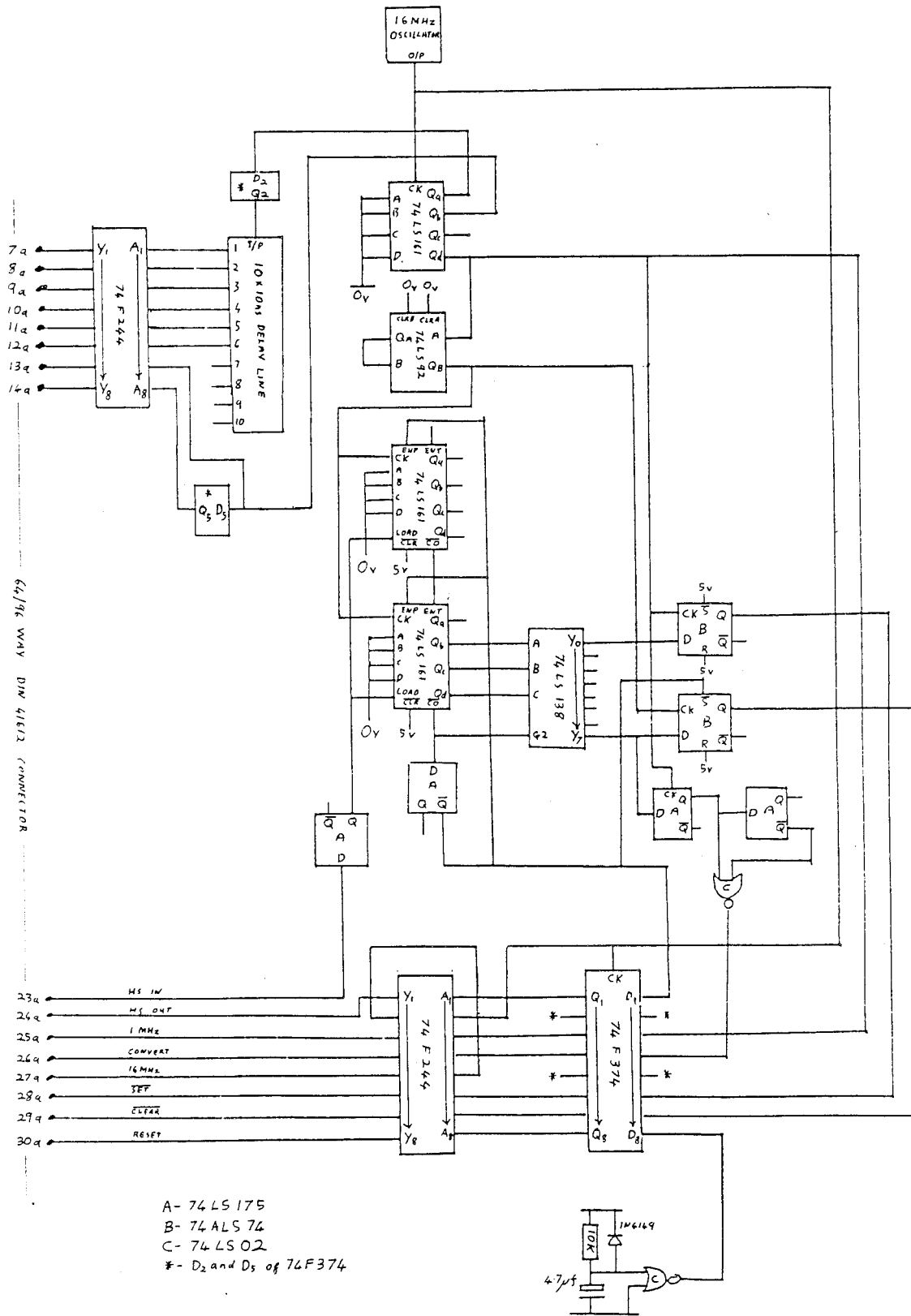
$$\cos\alpha = \frac{\begin{vmatrix} \text{Re}\{X\} & \text{Re}\{b\} \\ \text{Im}\{X\} & \text{Im}\{b\} \end{vmatrix}}{\begin{vmatrix} \text{Re}\{a\} & \text{Re}\{b\} \\ \text{Im}\{a\} & \text{Im}\{b\} \end{vmatrix}} \quad \cos\beta = \frac{\begin{vmatrix} \text{Re}\{a\} & \text{Re}\{X\} \\ \text{Im}\{a\} & \text{Im}\{X\} \end{vmatrix}}{\begin{vmatrix} \text{Re}\{a\} & \text{Re}\{b\} \\ \text{Im}\{a\} & \text{Im}\{b\} \end{vmatrix}} \quad (\text{III.24})$$

$$\sin\alpha = \frac{\begin{vmatrix} \text{Re}\{Y\} & \text{Re}\{b\} \\ \text{Im}\{Y\} & \text{Im}\{b\} \end{vmatrix}}{\begin{vmatrix} \text{Re}\{a\} & \text{Re}\{b\} \\ \text{Im}\{a\} & \text{Im}\{b\} \end{vmatrix}} \quad \sin\beta = \frac{\begin{vmatrix} \text{Re}\{a\} & \text{Re}\{Y\} \\ \text{Im}\{a\} & \text{Im}\{Y\} \end{vmatrix}}{\begin{vmatrix} \text{Re}\{a\} & \text{Re}\{b\} \\ \text{Im}\{a\} & \text{Im}\{b\} \end{vmatrix}} \quad (\text{III.25})$$

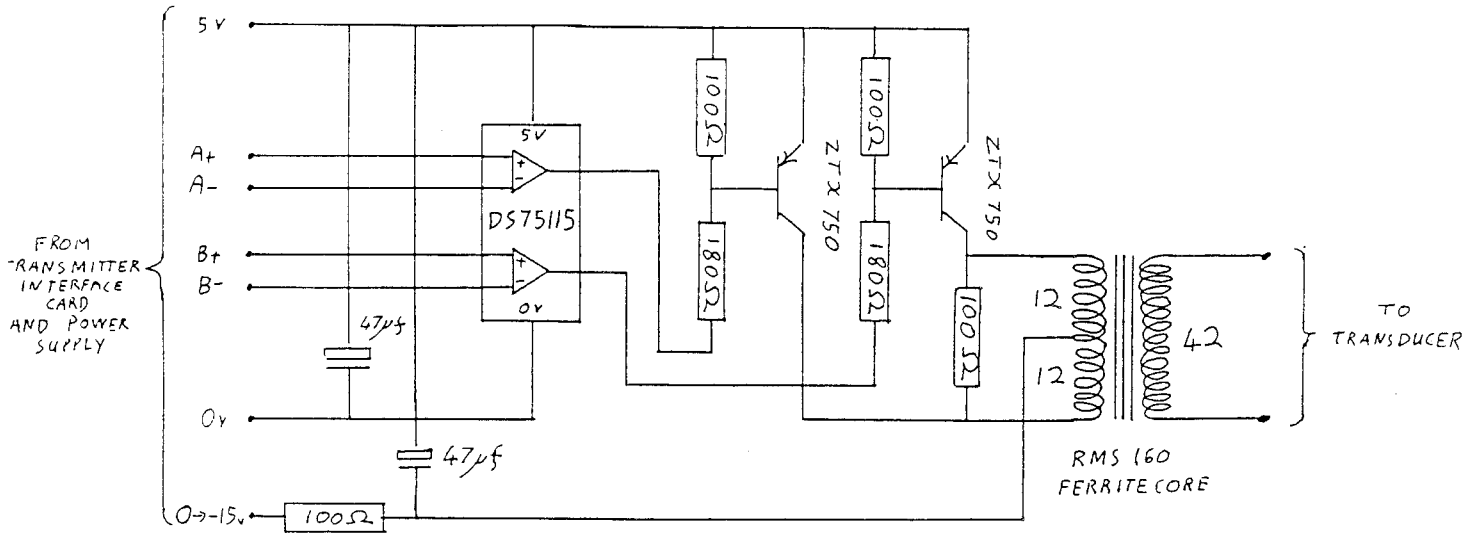
Hence α, β can be found in the correct quadrant.

Note that the solution is indeterminate if the waves are in phase at the wavegauge.

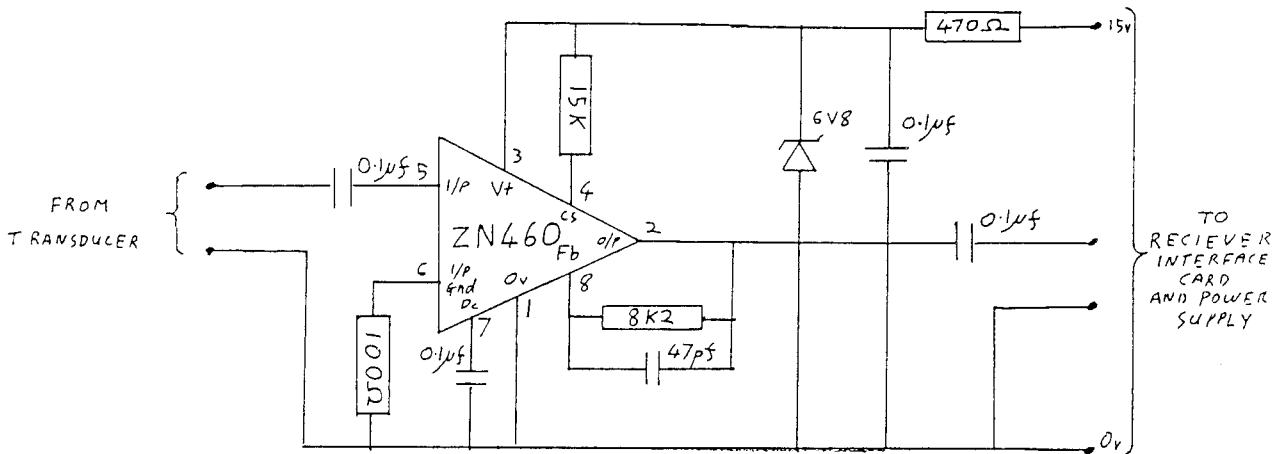
CIRCUIT DIAGRAMS



Bus timing control card



Transmitter driver circuit



Receiver preamplifier